

High-Pressure Torsion for Highly-Strained and High-Entropy Photocatalysts †

Saeid Akrami¹, Parisa Edalati¹, Masayoshi Fuji^{1,2*} and Kaveh Edalati^{3,4*}

¹ Department of Life Science and Applied Chemistry, Nagoya Institute of Technology, Japan

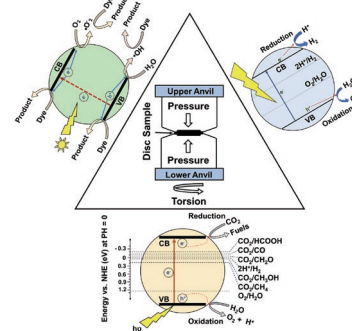
² Advanced Ceramics Research Center, Nagoya Institute of Technology, Japan

³ WPI International Institute for Carbon-Neutral Energy Research (WPI-I2CNER), Kyushu University, Japan

⁴ Mitsui Chemicals, Inc.- Carbon Neutral Research Center (MCI-CNRC), Kyushu University, Japan

Nowadays, the environmental crisis caused by using fossil fuels and CO₂ emissions has become a universal concern in people's life. Photocatalysis is a promising clean technology to produce hydrogen fuel, convert harmful components such as CO₂, and degrade pollutants like dyes in water. There are various strategies to improve the efficiency of photocatalysis so that it can be used instead of conventional methods, however, the low efficiency of the process has remained a big drawback. In recent years, high-pressure torsion (HPT), as a severe plastic deformation (SPD) method, has shown extremely high potential as an effective strategy to improve the activity of conventional photocatalysts and synthesize new and highly efficient photocatalysts. This method can successfully improve the activity by increasing the light absorbance, narrowing the bandgap, aligning the band structure, decreasing the electron-hole recombination, and accelerating the electron-hole separation by introducing large lattice strain, oxygen vacancies, nitrogen vacancies, high-pressure phases, heterojunctions, and high-entropy ceramics. This study reviews the recent findings on the improvement of the efficiency of photocatalysts by HPT processing and discusses the parameters that lead to these improvements.

Keywords: photocatalysis, water splitting, oxygen vacancy, nitrogen vacancy, heterojunctions, high-entropy alloys (HEAs), high-entropy ceramics



1. Introduction

Nowadays, serious environmental crises such as global warming and the formation of wastewater have forced humans to find alternatives like using clean fuels without carbon dioxide emissions such as hydrogen, reducing the pollutant gases such as carbon dioxide, and degrading the toxic pollutants in wastewater through clean strategies (Gaya and Abdullah, 2008). Using photocatalysts is an effective strategy to deal with these environmental crises using renewable sunlight energy (Ma et al., 2014). The function of photocatalysts is the acceleration of reduction and oxidation (redox) reactions under light irradiation. Reduction and oxidation reactions occur on the surface of a photocatalyst using the electrons and holes, respectively (Tong et al., 2012), to promote processes such as dye degradation (Akpan and Hameed, 2009), water splitting (Maeda, 2011), CO₂ conversion (Tu et al., 2014), etc.

In photocatalytic dye degradation, photoexcited

electrons take part in the degradation reaction of dyes (e.g. rhodamine B, methylene orange, acid red B, etc.) which normally exist in wastewaters produced by factories, laboratories and different industries (Akpan and Hameed, 2009). Photocatalytic water splitting includes the reduction to hydrogen and oxidation to oxygen (Maeda, 2011). In photocatalytic CO₂ conversion, photoexcited electrons contribute to the conversion of CO₂ to reactive and useful components such as carbon monoxide (CO), formic acid (HCOOH), formaldehyde (HCHO), methanol (CH₃OH) and methane (CH₄) (Tu et al., 2014). The mechanism of photocatalytic dye degradation, water splitting and CO₂ conversion is shown in Figs. 1(a), 1(b) and 1(c), respectively.

A photocatalyst should have some features to support the photocatalytic reactions including a narrow bandgap, appropriate band positions to cover the desired reactions, appropriate light absorbance, potential to absorb and activate the reactants, easy electron transition, and low recombination rate of electrons and holes (Akpan and Hameed, 2009; Maeda, 2011; Tu et al., 2014). Furthermore, high specific surface area, low cost, low toxicity and high stability are the other required properties that should be considered to select a photocatalyst (Tong et al., 2012). Challenging in this field is finding a photocatalyst

† Received 9 September 2022; Accepted 19 December 2022
J-STAGE Advance published online 25 March 2023

* Corresponding author: Masayoshi Fuji and Kaveh Edalati;

^{1,2} Add: 3-101-1 Hon-machi, Tajimi, Gifu 507-0033, Japan

^{3,4} Add: 744 Motoooka, Nishi-ku, Fukuoka 819-0395, Japan

E-mail: fuji@nitech.ac.jp (M.F.); kaveh.edalati@kyudai.jp (K.E.)

TEL: +81-572-27-6811 (M.F.); +81-92-802-6744 (K.E.)

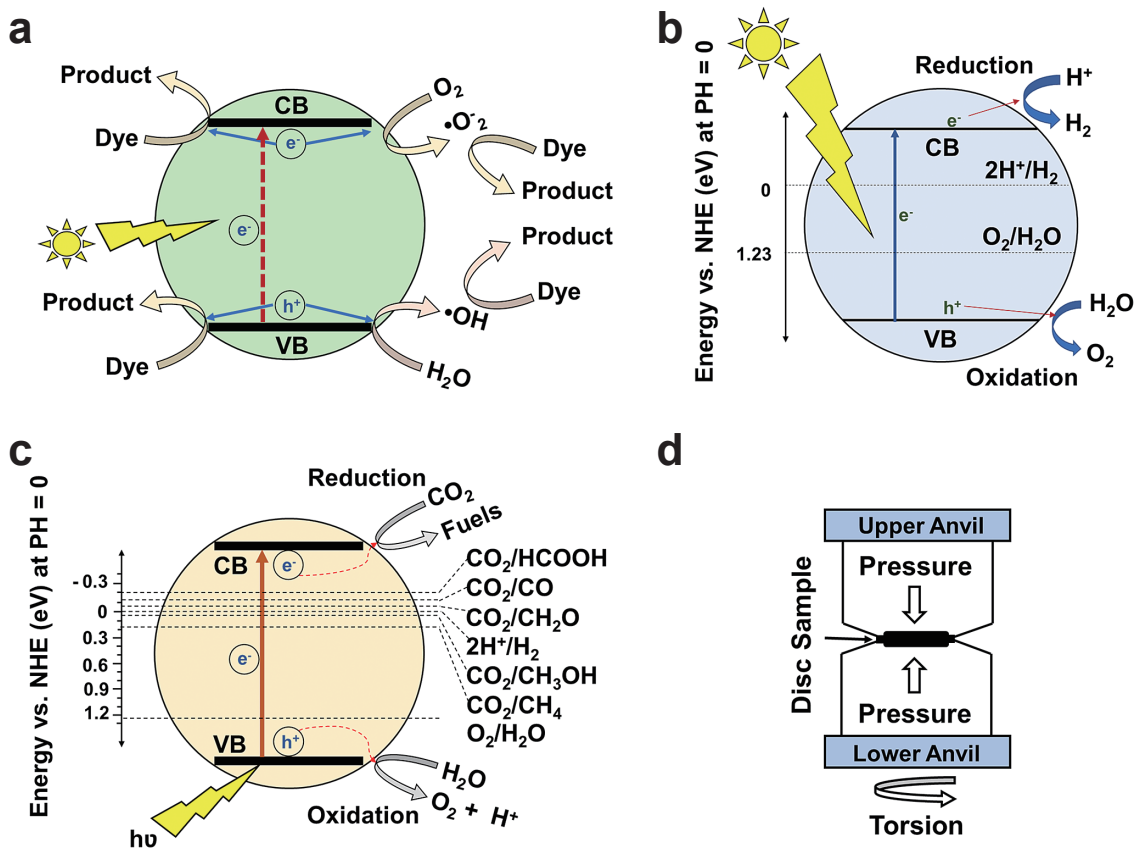


Fig. 1 Schematic illustration of (a) photocatalytic dye degradation, (b) photocatalytic water splitting, (c) photocatalytic CO_2 conversion, and (d) the HPT process.

with sufficient properties for considerable photocatalytic efficiency compared with the conventional catalytic processes. TiO_2 (Ajmal et al., 2014; Ni et al., 2007; Ola and Maroto-Valer, 2015), ZnO (Chakrabarti and Dutta, 2004; Lin et al., 2012; Zhao et al., 2019), $\text{g-C}_3\text{N}_4$ (Wen et al., 2017; Ye et al., 2015; Yuan et al., 2016), WO_3 (Liu Y. et al., 2010; Wang et al., 2012; Wang et al., 2019a), SrTiO_3 (Huang et al., 2014a; Iwashina and Kudo, 2011; Shan et al., 2017), GaN-ZnO (Hagiwara et al., 2017; Maeda et al., 2005; Ohno et al., 2012) and BiVO_4 (Gao et al., 2017; Sun et al., 2014; Zhou et al., 2010) are some of the most promising photocatalysts which have been utilized for photocatalytic dye degradation, water splitting and CO_2 conversion. The efficiencies of all these photocatalysts are still low for practical applications, and thus, various strategies were utilized to enhance the optical and structural properties and accordingly the photocatalytic activity of these materials.

Vacancy introduction (Huang et al., 2014b; Lei et al., 2014; Yu H. et al., 2019), strain engineering (Di J. et al., 2020; Feng et al., 2015; Sa et al., 2014), using mesoporous structures (Li Y. et al., 2010; Pauporté and Rathouský, 2007; Puangpetch et al., 2009), formation of heterojunctions (Cao et al., 2018; Moniz et al., 2015; Uddin et al., 2012), nanosheet production (Etman et al., 2018; Tu et al., 2012; Yu J. et al., 2010) and doping with impurities (Kuvarega

et al., 2011; Lee et al., 2016; Liu B. et al., 2018) are some of the reported methods which have been effective to improve the photocatalytic activity. Doping with impurities is the most common method which is used to improve the activity by narrowing the bandgap, but it usually causes recombination effects (Kuvarega et al., 2011).

High-pressure torsion (HPT) as one of the severe plastic deformation (SPD) methods has been introduced as an effective process to improve the photocatalytic efficiency of various materials by introducing vacancies (oxygen vacancy and nitrogen vacancy), dislocations, nanocrystals, lattice strain, heterojunctions, high-pressure phases and high-entropy ceramics. The HPT method is effective in reducing the recombination rate of electrons and holes which are usually observed in doped photocatalysts. The HPT method decreases the optical bandgap and enhances the photocatalytic activity of various oxides and oxynitrides including TiO_2 (Razavi-Khosroshahi et al., 2016b), ZnO (Razavi-Khosroshahi et al., 2017b), Al_2O_3 (Edalati et al., 2019b), MgO (Fujita et al., 2020a), ZrO_2 (Wang et al., 2020b), SiO_2 (Wang et al., 2020a), LiTaO_3 (Edalati et al., 2020a), CsTaO_3 (Edalati et al., 2020a), BiVO_4 (Akrami et al., 2022c), Ga_6ZnON_6 (Edalati et al., 2020b) for dye degradation, hydrogen production and CO_2 conversion. Furthermore, HPT was successfully used to synthesize new high-entropy oxides such as TiHfZrNbTaO_{11} (Edalati

et al., 2020c) and high-entropy oxynitrides such as $\text{TiZrHfNbTaO}_6\text{N}_3$ (Akrami et al., 2022a) for hydrogen production, oxygen evolution and CO_2 conversion. Moreover, it was also utilized to form heterojunctions in binary and high-entropy composites such as TiO_2 – ZnO (Hidalgo-Jimenez et al., 2020) and TiZrNbTaWO_{12} (Edalati et al., 2022b) to improve the photocatalytic activity for hydrogen and oxygen production.

In this review paper, the influence of the HPT method on optical properties, electronic structure, electron-hole separation, migration and recombination rates and photocatalytic efficiency of various photocatalysts is discussed. The improvement of photocatalytic activity of these materials for dye degradation, hydrogen production, oxygen production and CO_2 conversion is discussed by considering the generation of oxygen vacancies, nitrogen-vacancy complexes, high-pressure phases, heterojunctions and high-entropy ceramics.

2. High-pressure torsion (HPT)

The SPD process is typically used to form ultrafine-grained (UFG) and nanostructured materials with enhanced mechanical and functional properties (Estrin and Vinogradov, 2013; Valiev, 2004). SPD has various methods including HPT, introduced by Bridgman in 1935 for the first time (Bridgman, 1935). In this method, torsional strain under high pressure is applied to induce large plastic strain in various ranges of materials. In the HPT process, a disc-shape sample (Bridgman, 1935) that has typically a 10 mm diameter or a ring sample (Edalati and Horita, 2009) is inserted between two anvils under high pressure and strained by rotation of anvils against each other. A schematic illustration of HPT is shown in Fig. 1(d). The applied shear strain (γ) to the sample can be calculated by the following equation (Edalati and Horita, 2016).

$$\gamma = \frac{2\pi rN}{h} \quad (1)$$

where r , N and h are the distance from the center of the disc or ring, the number of turns and the sample height, respectively.

In addition to grain refinement, the HPT method is widely used for hardening of pure metals (Edalati and Horita, 2011; Starink et al., 2013), mechanical alloying of miscible and immiscible systems (Edalati et al., 2015b; Edalati, 2019a) and plastic deformation of hard-to-deform materials (Edalati et al., 2010a; Edalati et al., 2010b; Ikoma et al., 2012). Phase transformation, consolidation of powders, the introduction of defects such as oxygen vacancies and dislocations, narrowing of the bandgap and improvement of functionalities were frequently reported after HPT processing (Edalati, 2019d). The HPT method can be utilized for plastic deformation of oxides and ceramics which are hard and brittle materials at ambient temperature

(Edalati et al., 2022a). The presence of covalent or ionic bonding in ceramics results in their lower grain size after HPT processing compared to metals. Moreover, such bonding features result in the formation of large densities of defects such as vacancies and dislocations which can improve the properties and functionality of ceramics.

Despite the high potential of ceramics for various applications, there are some limited publications on the effect of HPT on the structure, properties and functionality of ceramics. A list of ceramics treated by HPT for various properties and applications and their relevant publications are given in Table 1. Table 1 indicates that these HPT-processed ceramics, including oxides, nitrides, oxynitrides and borides, have been investigated for photocatalysis, phase transformation, electrocatalysis, photocurrent generation, dielectric properties, bandgap narrowing, optical properties, mechanical properties, Li-ion batteries and microstructural features. Furthermore, the HPT method was also utilized to synthesize new ceramics for various applications. As can be seen in Table 1, ceramic photocatalysts processed or synthesized by HPT were used for water splitting (CsTaO_3 , LiTaO_3 , ZrO_2 , GaN-ZnO , TiO_2 – ZnO , TiO_2 , TiHfZrNbTaO_{11} , TiZrNbTaWO_{12} and $\text{TiZrHfNbTaO}_6\text{N}_3$), dye degradation (ZnO , MgO , $\gamma\text{-Al}_2\text{O}_3$ and SiO_2), CO_2 conversion (TiO_2 , BiVO_4 , TiHfZrNbTaO_{11} and $\text{TiZrHfNbTaO}_6\text{N}_3$) and oxygen production (TiZrNbTaWO_{12}).

3. Fundamentals and mechanism of photocatalysis

In photocatalysis, which is also called artificial photosynthesis, electrons in the valence band absorb the light photons, separate from the holes and transfer to the conduction band of the photocatalyst to form the electron-hole charge carriers. The charge carriers then migrate to the surface of the photocatalyst and finally take part in various chemical reactions. In this process, both reduction and oxidation reactions occur on the surface of the photocatalyst, provided that the thermodynamic and kinetic conditions are satisfied. From the thermodynamic point of view, a photocatalytic process will perform when the reduction and oxidation reaction potentials are between the valence band and the conduction band of a photocatalyst (Tong et al., 2012). For the reduction reactions, potentials lower than the valence band top are desirable, while for the oxidation reactions, potentials higher than the conduction band bottom are desirable. From the kinetic point of view, the electron-hole separation should be fast, and their recombination should be slow. Here, the fundamentals of three main photocatalytic reactions are mentioned.

3.1 Photocatalytic dye degradation

In photocatalytic dye degradation, there are two direct and indirect pathways. In the direct pathway, the dye

Table 1 Summary of major publications about ceramics treated by HPT and their major applications or features.

Materials	Investigated properties and application	Reference
<i>Photocatalysis</i>		
TiHfZrNbTaO ₁₁	Photocatalytic activity for CO ₂ conversion	(Akrami et al., 2022b)
TiZrHfNbTaO ₆ N ₃	Photocatalytic activity for CO ₂ conversion	(Akrami et al., 2022a)
BiVO ₄	Photocatalytic activity for CO ₂ conversion	(Akrami et al., 2022c)
TiO ₂ -II	Photocatalytic activity for CO ₂ conversion	(Akrami et al., 2021b)
MgO	Photocatalytic activity for dye degradation	(Fujita et al., 2020a)
SiO ₂	Photocatalytic activity for dye degradation	(Wang et al., 2020a)
γ-Al ₂ O ₃	Photocatalytic activity for dye degradation	(Edalati et al., 2019b)
ZnO	Photocatalytic activity for dye degradation	(Razavi-Khosroshahi et al., 2017b)
TiZrHfNbTaO ₆ N ₃	Photocatalytic activity for hydrogen production	(Edalati et al., 2021)
ZrO ₂	Photocatalytic activity for hydrogen production	(Wang et al., 2020b)
CsTaO ₃ , LiTaO ₃	Photocatalytic activity for hydrogen production	(Edalati et al., 2020a)
GaN–ZnO	Photocatalytic activity for hydrogen production	(Edalati et al., 2020b)
TiHfZrNbTaO ₁₁	Photocatalytic activity for hydrogen production	(Edalati et al., 2020c)
TiO ₂ –ZnO	Photocatalytic activity for hydrogen production	(Hidalgo-Jimenez et al., 2020)
TiO ₂ -II	Photocatalytic activity for hydrogen production	(Razavi-Khosroshahi et al., 2016b)
TiZrNbTaWO ₁₂	Photocatalytic activity for oxygen production	(Edalati et al., 2022b)
<i>Reviews</i>		
Oxides	Review on HPT of oxides	(Edalati, 2019b)
	Review on HPT	(Edalati and Horita, 2016)
<i>Phase transformation</i>		
SiO ₂ , VO ₂	Phase transformation	(Edalati et al., 2019a)
TiO ₂	Grain coarsening and phase transformation	(Edalati et al., 2019c)
ZrO ₂	Phase transformation by ball milling and HPT	(Delogu, 2012)
ZrO ₂	Allotropic phase transformations	(Edalati et al., 2011)
TiO ₂	Plastic strain and phase transformation	(Razavi-Khosroshahi et al., 2016a)
BN	FEM modeling of plastic flow and strain-induced phase transformation	(Feng et al., 2019)
BN	Coupled elastoplasticity and plastic strain-induced phase transformation	(Feng and Levitas, 2017)
<i>Electrocatalysis</i>		
TiO ₂ -II	Electrocatalysis for hydrogen generation	(Edalati et al., 2019c)
<i>Photocurrent</i>		
Bi ₂ O ₃	Enhanced photocurrent generation	(Fujita et al., 2020b)
TiO ₂ -II	Visible light photocurrent generation	(Wang et al., 2020c)
<i>Dielectric properties</i>		
BaTiO ₃	Optical and dielectric properties	(Edalati et al., 2015a)
CuO	Dielectric properties	(Makhnev et al., 2011)
<i>Bandgap investigation</i>		
ZnO	Bandgap narrowing	(Qi et al., 2021)
<i>Optical properties</i>		
Y ₂ O ₃	Optical properties	(Razavi-Khosroshahi et al., 2017a)
CuO, Y ₃ Fe ₅ O ₁₂ , FeBO ₃	Optical properties and electronic structure	(Gizhevskii et al., 2011)
Cu ₂ O, CuO	Middle infrared absorption and X-ray absorption	(Mostovshchikova et al., 2012)
CuO, Y ₃ Fe ₅ O ₁₂ , FeBO ₃	Optical properties	(Telegin et al., 2012)
<i>Mechanical properties</i>		
α-Al ₂ O ₃	Microstructure and mechanical properties	(Edalati and Horita, 2010)
Fe _{53.3} Ni _{26.5} B _{20.2} Co _{28.2} Fe _{38.9} Cr _{15.4} Si _{0.3} B _{17.2}	Microstructure and mechanical properties	(Permyakova and Glezer, 2020)
<i>Lithium-ion batteries</i>		
Fe ₃ O ₄	Lithium-ion batteries	(Qian et al., 2018)
<i>Microstructural features</i>		
ZnO	Plastic flow and microstructural instabilities	(Qi et al., 2018)
YBa ₂ Cu ₃ O _y	Microstructural investigation	(Kuznetsova et al., 2017)
Fe _{71.2} Cr _{22.7} Mn _{1.3} N _{4.8}	Microstructural features	(Shabashov et al., 2018)

degrades directly by the excited electrons and holes in the conduction band and the valence band, respectively, as shown in Fig. 1(a). In the indirect pathway, which is more conventional than the direct pathway, the electrons in the conduction band react with the O_2 to produce the $O_2^{\cdot-}$ radicals. The $O_2^{\cdot-}$ radicals then react with the dye to form the reduction products (Li X. et al., 2018). In the valence band, holes react with H_2O to produce $\cdot OH$, and the $\cdot OH$ radicals react with the dye to produce the oxidation products as shown in Fig. 1(a).

3.2 Photocatalytic water splitting

In photocatalytic water splitting, electrons in the conduction band take part in the reduction reaction to produce H_2 , while holes in the valence band take part in the oxidation reaction to produce O_2 (Lu et al., 2021), as shown in Fig. 1(b). In most photocatalysts, overall water splitting does not occur, and the process is limited to either reduction or oxidation reactions thus a sacrificial agent or scavenger is usually required to produce electrons or holes. Methanol and $AgNO_3$ are popular sacrificial agents for photocatalytic hydrogen and oxygen production, respectively.

3.3 Photocatalytic CO_2 conversion

In photocatalytic CO_2 conversion, electrons in the conduction band along with protons (H^+) produced from water oxidation in the valence band, take part in various reduction reactions leading to the formation of CO , CH_4 and some other hydrocarbons as shown in Fig. 1(c). The first step in photocatalytic CO_2 conversion is the adsorption of CO_2 molecules on the surface of the photocatalyst which occurs in three modes including oxygen coordination, carbon coordination and mixed coordination

(Lu et al., 2021), as shown in Fig. 2. These CO_2 adsorption modes determine the reaction pathway for photocatalytic CO_2 conversion. For instance, the oxygen coordination mode, with the bidentate bonding of oxygen atoms with the surface of the photocatalyst, leads to the fabrication of formate anions as an intermediate product and formic acid as the final product. In the carbon coordination mode, with the monodentate binding of carbon and photocatalyst surface, the reaction results in carboxyl radical production. After the adsorption step of CO_2 to the surface of the photocatalyst, the conversion reactions occur via different pathways.

It was reported that there are three main pathways for CO_2 photoreduction: (i) carbene pathway (ii) formaldehyde pathway and (iii) glyoxal pathway (Habisreutinger et al., 2013; Maeda and Domen, 2007; Wang et al., 2021). The reactions for these three pathways are presented in Table 2. In all these pathways, the $CO_2^{\cdot-}$ radical is the main intermediate product which is formed by the reaction of

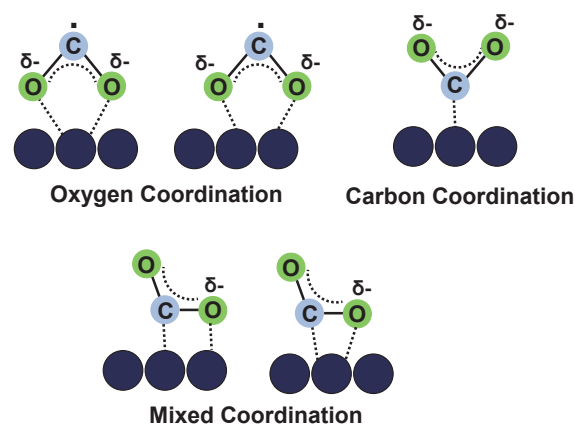


Fig. 2 CO_2 adsorption modes on the surface of photocatalysts.

Table 2 CO_2 photoreduction pathways (Habisreutinger et al., 2013).

Carbene Pathway	Formaldehyde Pathway	Glyoxal Pathway
(1) $CO_2 + e^- \rightarrow CO_2^{\cdot-}$	(1) $CO_2 + e^- \rightarrow CO_2^{\cdot-}$	(1) $CO_2 + e^- \rightarrow CO_2^{\cdot-}$
(2) $CO_2^{\cdot-} + e^- + H^+ \rightarrow CO + OH^-$	(2) $CO_2^{\cdot-} + H^+ \rightarrow \cdot COOH$	(2) $CO_2^{\cdot-} + e^- + H^+ \rightarrow CHOO^-$
(3) $CO + e^- \rightarrow CO^{\cdot-}$	(3) $\cdot COOH + e^- + H^+ \rightarrow HCOOH$	(3) $CHOO^- + H^+ \rightarrow HCOOH$
(4) $CO^{\cdot-} + e^- + H^+ \rightarrow C + OH^-$	(4) $HCOOH + e^- + H^+ \rightarrow H_3OOC^{\cdot}$	(4) $HCOOH + e^- \rightarrow HOC^{\cdot}$
(5) $C + e^- + H^+ \rightarrow CH^{\cdot}$	(5) $HCOOH_2 + e^- + H^+ \rightarrow HCOH + H_2O$	(5) $HOC^{\cdot} + OH^- \rightarrow C_2H_2O_2$
(6) $CH^{\cdot} + e^- + H^+ \rightarrow CH_2$	(6) $HCOH + e^- \rightarrow H_2C^{\cdot}O^-$	(6) $C_2H_2O_2 + e^- + H^+ \rightarrow H_3O_2C_2^{\cdot}$
(7) $CH_2 + e^- + H^+ \rightarrow CH_3^{\cdot}$	(7) $H_2C^{\cdot}O^- + H^+ \rightarrow H_2OHC^{\cdot}$	(7) $H_3O_2C_2^{\cdot} + e^- + H^+ \rightarrow C_2H_4O_2$
(8) $CH_3^{\cdot} + e^- + H^+ \rightarrow CH_4$	(8) $H_2OHC^{\cdot} + e^- + H^+ \rightarrow CH_3OH$	(8) $C_2H_4O_2 + e^- + H^+ \rightarrow H_3OC_2^{\cdot} + H_2O$
(9) $CH_3^{\cdot} + OH^- \rightarrow CH_3OH$	(9) $CH_3OH + e^- + H^+ \rightarrow \cdot CH_3 + H_2O$	(9) $H_3OC_2^{\cdot} + e^- + H^+ \rightarrow C_2H_4O$
	(10) $\cdot CH_3 + e^- + H^+ \rightarrow CH_4$	(10) $C_2H_4O + h^+ \rightarrow H_3OC_2^{\cdot} + H^+$
		(11) $H_3OC_2^{\cdot} \rightarrow CH_3 + CO$
		(12) $CH_3^{\cdot} + e^- + H^+ \rightarrow CH_4$

adsorbed CO_2 and an electron. In the carbene pathway, CO_2^- converts to CO^\bullet and leads to the production of CO , CH_2 , CH_4 and CH_3OH . In this pathway, carbon coordination is the main binding mode. In the formaldehyde pathway, CO_2^- converts to $^\bullet\text{COOH}$ to produce HCOOH , CH_3OH and CH_4 . In this pathway, CO_2^- attaches to the catalyst by monodentate or bidentate binding. In monodentate binding, either one oxygen atom in CO_2^- or one carbon atom in CO_2^- are bonded to the surface of the photocatalyst. In the bidentate mode, both oxygen atoms in CO_2^- are bonded to the photocatalyst surface. In the glyoxal pathway, C_2 components are formed by some complicated reactions, though there are limitations to producing C_2 due to the low selectivity of the photocatalyst. In this pathway, CO_2^- converts to the formyl radical HOC^\bullet to form $\text{C}_2\text{H}_2\text{O}_2$, $\text{C}_2\text{H}_4\text{O}_2$, $\text{C}_2\text{H}_4\text{O}$, CO and CH_4 . In all these pathways, CO_2 adsorption and activation are key parameters to adjust the selectivity of photocatalysts and this should be empowered by some strategies such as oxygen vacancy generation and strain engineering (Fu et al., 2020).

4. Impact of HPT on photocatalysis

As given in Table 1, numerous studies in recent years reported that the HPT method can be used to improve the photocatalytic activity of ceramics. Bandgap narrowing for the easier transition of photoexcited electrons from the valence band to the conduction band, increasing the light absorbance in the visible region of light, electronic band structure alignment, decreasing the recombination rate of electrons and holes and accelerating the electron-hole separation and migration are some phenomena responsible for the high activity of photocatalysts processed or synthesized by HPT. The occurrence of these phenomena was attributed to the formation of oxygen vacancies, nitrogen-vacancy complexes, high-pressure phases, heterojunctions and high-entropy phases which will be discussed in detail as follows.

4.1 Generation of oxygen vacancies

Oxygen vacancies on the surface have a significant effect on the photocatalytic activity of materials, since they can act as active sites to adsorb and activate the reactants and as trap sites for photoexcited electrons. In contrast, oxygen vacancies in the bulk of photocatalysts may act as recombination centers and lead to decreasing photocatalytic efficiency. Oxygen vacancies can also reduce the optical bandgap by changing the electronic structure of materials via the formation of defect states between the valence band and the conduction band. The formation of oxygen vacancies after HPT processing has been evidenced by several analysis methods such as electron paramagnetic resonance (EPR), X-ray photoelectron spectroscopy (XPS), Raman spectroscopy, differential scanning calorimetry (DSC), and X-ray diffraction (XRD) (Fujita et al., 2020a;

Razavi-Khosroshahi et al., 2016b; Wang et al., 2020a). Furthermore, changing the color of catalysts to the darker ones, which are frequently observed after HPT processing, indicates the light absorbance in the visible region due to the formation of oxygen vacancies as color centers (Fujita et al., 2020b; Razavi-Khosroshahi et al., 2017b; Wang et al., 2020b). Among the photocatalysts treated by HPT, Al_2O_3 (Edalati et al., 2019b), MgO (Fujita et al., 2020a), ZrO_2 (Wang et al., 2020b), SiO_2 (Wang et al., 2020a), LiTaO_3 (Edalati et al., 2020a), CsTaO_3 (Edalati et al., 2020a) and BiVO_4 (Akrami et al., 2022c) are oxides which exhibited enhanced photocatalytic activity by oxygen vacancy formation.

Al_2O_3 : Al_2O_3 is an insulator with a large bandgap (~ 9 eV) and does not show photocatalytic activity. First-principles calculations suggested that the formation of oxygen vacancies can reduce the optical bandgap of Al_2O_3 even to the visible light region (Edalati et al., 2019b). The application of HPT to Al_2O_3 resulted in the formation of oxygen vacancies, the reduction of optical bandgap and its photocatalytic activity. The formation of oxygen vacancies after HPT is shown in Fig. 3(a) using DSC analysis by the appearance of a peak at 530 K. After the HPT process, a narrow bandgap of 2.5 eV was achieved, in good agreement with the first-principles calculations, and the material showed photocatalytic activity for rhodamine B dye degradation under UV irradiation with an activity comparable to TiO_2 (Fig. 3(b)).

MgO : MgO , as another ceramic insulator, also exhibited high light absorbance and bandgap narrowing (from 7.8 eV to 3.9 eV) after HPT processing (Fujita et al., 2020a). The HPT-processed MgO showed photocatalytic activity for methylene blue dye degradation under UV irradiation (55 % decomposition after 3 h). The formation of oxygen vacancies in this material was evidenced by XPS analysis of Mg 2p, which showed a shift to lower energy, and such a shift became more significant by increasing the applied shear strain (i.e. by increasing the number of HPT turns).

ZrO_2 : ZrO_2 is another ceramic that was processed by HPT to introduce a high concentration of oxygen vacancies (Wang et al., 2020b). The optical bandgap of this material decreased from 5.1 to 4.0 eV due to the formation of oxygen vacancies after HPT. The formation of oxygen vacancies after HPT processing at various temperatures is shown in Fig. 3(c) using the EPR analysis. The appearance of a pair peak with a g factor of ~ 2 indicates the formation of oxygen vacancies, while the formation of oxygen vacancies is enhanced by increasing the HPT processing temperature. Improvement of photocatalytic activity of ZrO_2 using HPT for hydrogen evolution is shown in Fig. 3(d), indicating that the photocatalytic activity is improved by increasing the concentration of oxygen vacancies.

SiO_2 : SiO_2 quartz sand also was examined for photocatalytic activity after processing using the HPT method

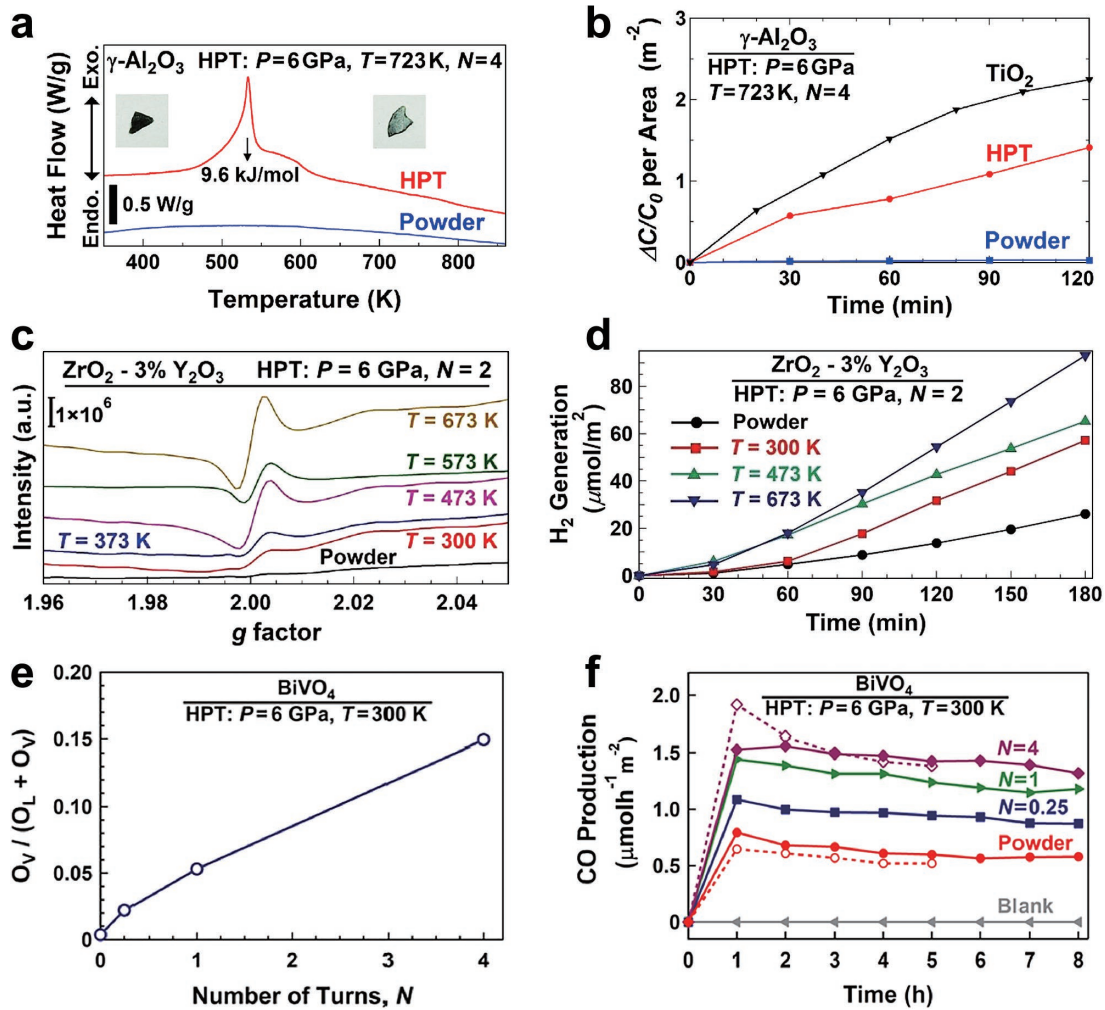


Fig. 3 Formation of oxygen vacancies achieved by HPT processing and improvement of photocatalytic activity. (a) DSC analysis and (b) photocatalytic rhodamine B degradation for $\gamma\text{-Al}_2\text{O}_3$ before and after HPT processing compared with TiO_2 (Edalati et al., 2019b). (c) EPR spectra and (d) corresponding photocatalytic hydrogen production for $\text{ZrO}_2\text{-}3\% \text{Y}_2\text{O}_3$ before and after HPT processing at 300, 437, 573 and 673 K (Wang et al., 2020b). (e) Oxygen vacancy concentration and (f) photocatalytic CO_2 to CO conversion for BiVO_4 before and after HPT processing for $N = 0.25, 1$ and 4 turns (Akrami et al., 2022c). Copyright: (2019) Elsevier, (2020) Royal Society of Chemistry, (2022) Elsevier.

(Wang et al., 2020a). This material with the initially reported bandgap of ~ 9 eV and negligible light absorbance exhibited a bandgap narrowing to 2.8 eV, with a small activity for rhodamine B dye degradation under UV light irradiation.

LiTaO₃ and CsTaO₃: LiTaO₃ and CsTaO₃ are two tantalate perovskites that show activity for photocatalytic hydrogen production. After oxygen vacancy generation by HPT processing, both materials exhibited bandgap narrowing (4.7 to 4.2 eV for LiTaO₃ and 4.7 to 3.6 eV for CsTaO₃) and enhanced photocatalytic activity for hydrogen generation (Edalati et al., 2020a).

BiVO₄: BiVO₄ is a popular photocatalyst for CO_2 conversion due to its low bandgap, but it suffers from a high recombination rate of electrons and holes and a low position of the conduction band. HPT could successfully solve these two problems by simultaneously introducing the oxygen vacancies and lattice strain (Akrami et al.,

2022c). Increasing the oxygen vacancy concentration by increasing the number of HPT turns, calculated from XPS, is shown in Fig. 3(e). These structural modifications by HPT processing resulted in significant improvement of photocatalytic CO_2 conversion on BiVO₄, as shown in Fig. 3(f).

4.2 Generation of nitrogen-vacancy complexes

Oxynitrides are promising photocatalysts due to their low bandgap compared with oxide photocatalysts. It was reported that nitrogen vacancies, which are formed during the synthesis of these materials, can act as recombination centers, and reduce photocatalytic activity (Maeda and Domen, 2007). However, it was observed that HPT processing of Ga_6ZnON_6 led to the formation of nitrogen-based vacancies, decreasing the electron and hole recombination and enhancement of photocatalytic activity (Edalati et al., 2020b). Fig. 4(a) shows the EPR spectra of

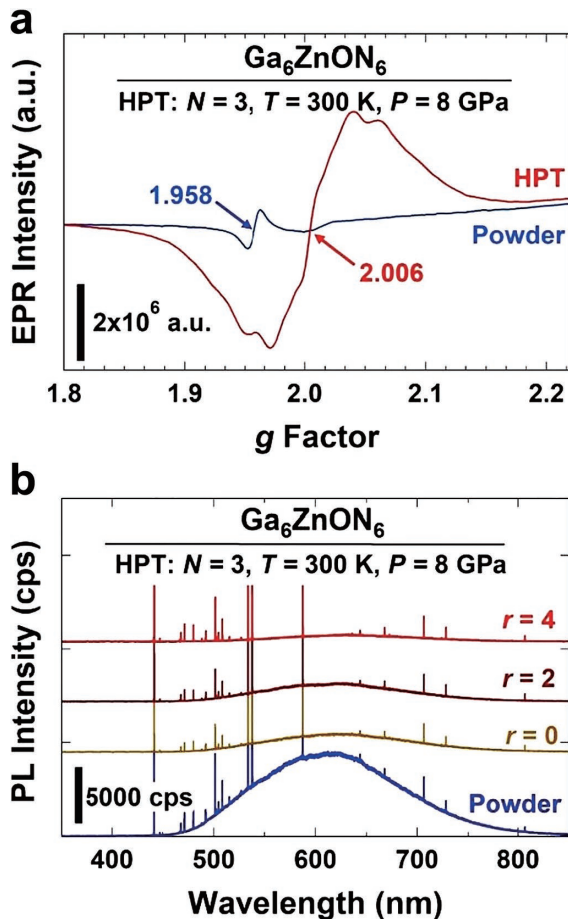


Fig. 4 Formation of nitrogen-based vacancy complexes and suppression of recombination in oxynitride processed by HPT. (a) EPR spectra and (b) photoluminescence spectra for Ga_6ZnON_6 before and after HPT processing (r : radial distance from center of HPT-processed disc) (Edalati et al., 2020b). Copyright: (2020) Elsevier.

Ga_6ZnON_6 before and after HPT processing. A g factor of 1.958 for powder is a piece of evidence for the formation of nitrogen monovacancies during the synthesis of oxynitrides, while a g factor of 2.006 indicates the presence of nitrogen-based vacancy complexes by HPT processing. Introducing the nitrogen-based vacancy complexes to this material by HPT, led to reducing the bandgap from 2.7 eV to 2.4 eV, enhancing the light absorbance and improvement of photocatalytic hydrogen production under UV irradiation. This study showed that in addition to the location of vacancies (surface or bulk), their arrangement (monovacancy or vacancy complex) can affect photocatalytic activity. These vacancy complexes can act as active sites for reactions rather than the recombination centers for electrons and holes. Decreasing the recombination of electrons and holes after HPT processing for this oxynitride is presented in Fig. 4(b), in which the photoluminescence intensity is suppressed effectively after the HPT process.

4.3 Formation of high-pressure phases

Due to high pressure and high strain in HPT, the method

can lead to the formation of metastable and high-pressure phases. These phases usually form with fast kinetics at lower pressures during HPT processing compared to the transition pressures under static conditions due to the presence of high concentrations of nanograin boundaries and defects. It was suggested that the formation of these defects and their interaction increase localized pressure and result in the formation and stability of high-pressure phases (Edalati, 2019b). BaTiO_3 (tetragonal to cubic) (Makhnev et al., 2011), TiO_2 (anatase-tetragonal to orthorhombic TiO_2 -II) (Razavi-Khosroshahi et al., 2016b), Y_2O_3 (cubic to monoclinic) (Razavi-Khosroshahi et al., 2017a), ZnO (wurtzite-hexagonal to rocksalt-cubic) (Razavi-Khosroshahi et al., 2017b) and SiO_2 (quartz to coesite) (Wang et al., 2020a) are some oxides which showed transition to high-pressure phases after HPT processing. Among these materials, the formation of high-pressure phases in TiO_2 and ZnO was reported to lead to the improvement of photocatalytic activity for hydrogen production, CO_2 conversion and dye degradation. Figs. 5(a) and 5(b) illustrate the pressure-temperature phase diagrams of TiO_2 and ZnO , respectively; Figs. 5(c) and 5(d) show the formation of TiO_2 -II and rocksalt- ZnO high-pressure phases after HPT processing, respectively; and Figs. 5(c) and 5(d) show the influence of HPT processing on the enhancement of the photocatalytic activity of TiO_2 and ZnO , respectively. Since TiO_2 and ZnO are the most common photocatalysts, the reports on the application of HPT to these two photocatalysts are of significance as they suggested new solutions to enhance the activity by nanostructure and polymorphic control and without dopant or impurity addition (Razavi-Khosroshahi et al., 2016b; Razavi-Khosroshahi et al., 2017b).

TiO_2 : TiO_2 light absorbance improved significantly after the formation of the high-pressure TiO_2 -II (columbite) phase by HPT processing (Akrami et al., 2021b; Razavi-Khosroshahi et al., 2016b). The color of TiO_2 changed from white to gray or green and its bandgap decreased from 3.1 eV to 2.5 eV, which resulted in photocatalytic activity of the material under visible light. To solve the recombination issue due to the presence of bulk defects after HPT processing, the HPT-processed sample was processed by annealing which resulted in a further increase in the photocatalytic activity and photocurrent generation. It was shown that the formation of TiO_2 -II results in photocatalytic activity for hydrogen production under visible light and CO_2 conversion under UV light (Fig. 5(e)), although the high activity is influenced by other factors such as the presence of oxygen vacancies and interphase boundaries.

ZnO : HPT processing of ZnO led to the formation of a high-pressure rocksalt phase and accordingly to the improvement of light absorbance in the visible region with a bandgap narrowing from 3.0 eV to 1.8 eV (Razavi-

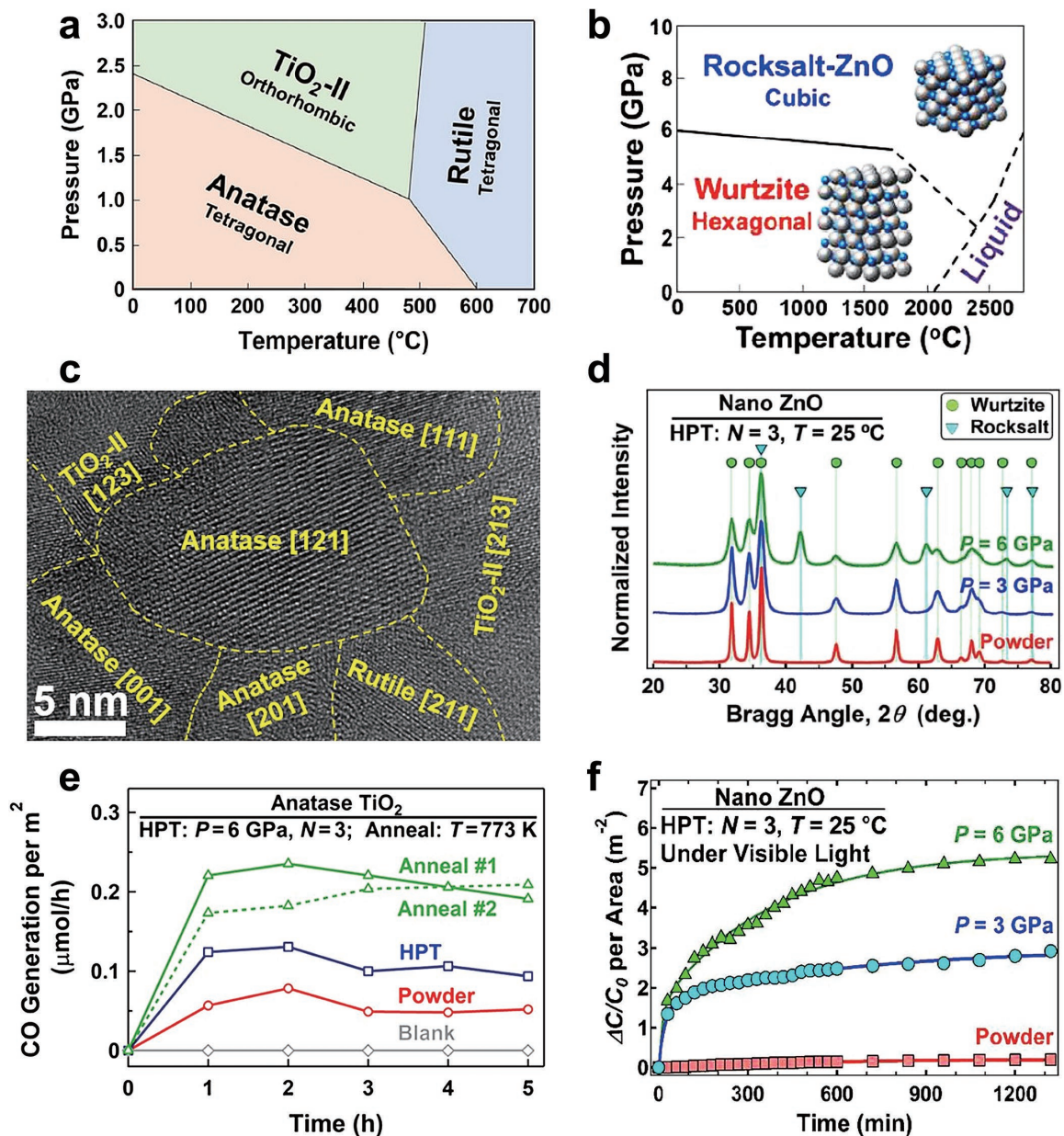


Fig. 5 Improved photocatalytic activity by introducing high-pressure phases. (a) Phase diagram of TiO_2 (Akrami et al., 2021b), (b) phase diagram of ZnO (Razavi-Khosroshahi et al., 2017b), (c) high-resolution lattice image of TiO_2 including TiO_2 -II high-pressure phase (Akrami et al., 2021b), (d) XRD profile of ZnO including rocksalt high-pressure phase (Razavi-Khosroshahi et al., 2017b), (e) photocatalytic CO_2 conversion on TiO_2 before and after HPT processing and after annealing under UV light (Akrami et al., 2021b), and (f) photocatalytic rhodamine B dye degradation for ZnO before and after HPT processing under visible light (Razavi-Khosroshahi et al., 2017b). Copyright: (2021) Elsevier, (2017) Royal Society of Chemistry.

Khosroshahi et al., 2017b). This bandgap narrowing was also predicted by first-principles calculations. The HPT-processed ZnO, containing a high-pressure phase with a large fraction of oxygen vacancies and interphase boundaries, showed photocatalytic rhodamine B dye degradation under visible light, while its activity improved with increasing the processing pressure (Fig. 5(f)).

4.4 Formation of heterojunctions

Heterojunctions are the space-charge regions that are formed by the combination of two different phases or different semiconductors. Charge carriers can penetrate

heterojunctions which results in the formation of an electronic field in this region (Moniz et al., 2015). Heterojunctions accelerate the electron and hole separation and improve their migration to the surface of the photocatalyst for the reactions. Furthermore, they significantly suppress recombination (Cao et al., 2018; Uddin et al., 2012). As mentioned earlier, among HPT-processed materials, some of them exhibit phase transformation resulting in the formation of heterojunctions between two or more phases such as cubic-rhombohedral phases in Al_2O_3 (Edalati et al., 2019b), monoclinic-tetragonal phases in ZrO_2 (Wang et al., 2020b) and coesite-quartz

phases in SiO_2 . (Wang et al., 2020a). There is also an application of HPT to TiO_2 -ZnO composite to generate heterojunctions for enhanced photocatalytic hydrogen production (Hidalgo-Jimenez et al., 2020). There is another attempt to generate 10 different heterojunctions in a high-entropy oxide TiZrNbTaWO_{12} for visible-light-driven photocatalytic oxygen production (Edalati et al., 2022b). In all these cases, the interphase boundaries formed by HPT can act as sites to accelerate the electron-hole separation to effectively improve the photocatalytic activity, as will be discussed below for the TiO_2 -ZnO composite.

TiO_2 -ZnO: A recent study generated heterojunctions

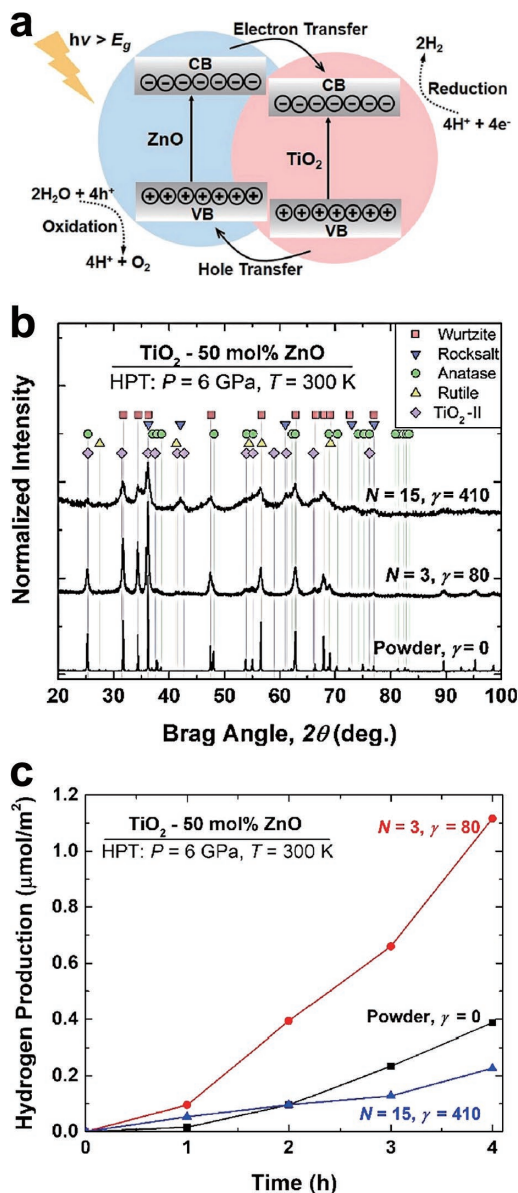


Fig. 6 Enhanced photocatalytic hydrogen production by heterojunction formation. (a) Schematic illustration of electronic band structure of TiO_2 -ZnO composite including heterojunctions. (b) XRD profile and (c) photocatalytic hydrogen production on TiO_2 -ZnO composite before and after HPT processing for $N = 3$ and 15 turns (Hidalgo-Jimenez et al., 2020). Copyright: (2020) Elsevier.

using HPT by making a composite of TiO_2 and ZnO as two typical catalysts for photocatalytic hydrogen production (Hidalgo-Jimenez et al., 2020). This work was performed to ease electron-hole separation as shown in Fig. 6(a). In addition to TiO_2 -ZnO heterojunctions, HPT processing led to the formation of high-pressure phases and formation of various kinds of heterojunctions. XRD profiles of TiO_2 -ZnO composite show the presence of five different phases of TiO_2 and ZnO in Fig. 6(b). After HPT processing, the light absorbance of the composite significantly increased in the visible light region and a bandgap narrowing was observed from 3.2 eV to 2.6 eV and 1.6 eV for $N = 3$ and 15 HPT turns, respectively. The recombination rate of electrons and holes was also suppressed effectively after HPT processing. Although electronic structure, light absorbance and recombination suppression improved by increasing the number of HPT turns to $N = 15$, photocatalytic hydrogen production for $N = 15$ was lower compared to the powder mixture and sample processed by $N = 3$ due to the formation of very small crystals and poor crystallinity (Fig. 6(c)). The composite processed with $N = 3$ had a hydrogen production amount of 2.5 time better than initial powders mixture under UV irradiation.

4.5 Production of high-entropy ceramics

High-entropy ceramics are materials with at least five principal cations and a mixing entropy higher than $1.5R$ (R : gas constant) (Akrami et al., 2021a; Oses et al., 2020). These materials have been employed for various applications due to their high stability, lattice strain, inherent defects and high entropy of mixing (Zhang and Reece, 2019; Xiang et al., 2021). They have potential to be used as Li-ion batteries (Lun et al., 2021; Nguyen et al., 2020; Wang et al., 2019b), catalysts (Albedwawi et al., 2021; Qiao et al., 2021; Xu et al., 2020), photocatalysts (Akrami et al., 2022a; Akrami et al., 2022b; Edalati et al., 2020c), supercapacitors (Jin et al., 2018; Liang et al., 2020; Talluri et al., 2021), dielectrics (Bérardan et al., 2016; Zhou et al., 2020; Zhou et al., 2022), thermal barrier coatings (Li F. et al., 2019; Ren et al., 2020; Zhang et al., 2022), etc. Utilizing the high-entropy ceramics as photocatalysts, which was performed for the first time by the authors of the current work, is a new functional aspect of these materials which is in its initial research stage. The high stability of high-entropy ceramics and the formation of defects and strain in these materials were the main motivations to use them as photocatalysts. As will be discussed below, the oxides TiZrHfNbTaO_{11} and TiZrNbTaWO_{12} and the oxynitride $\text{TiZrHfNbTaO}_6\text{N}_3$ are high-entropy ceramics synthesized by HPT and used for photocatalytic hydrogen production, CO_2 conversion and O_2 evolution. Since oxides and oxynitrides with d^0 and d^{10} electronic configurations show good photocatalytic activity, five d^0 cations were selected to design these photocatalysts.

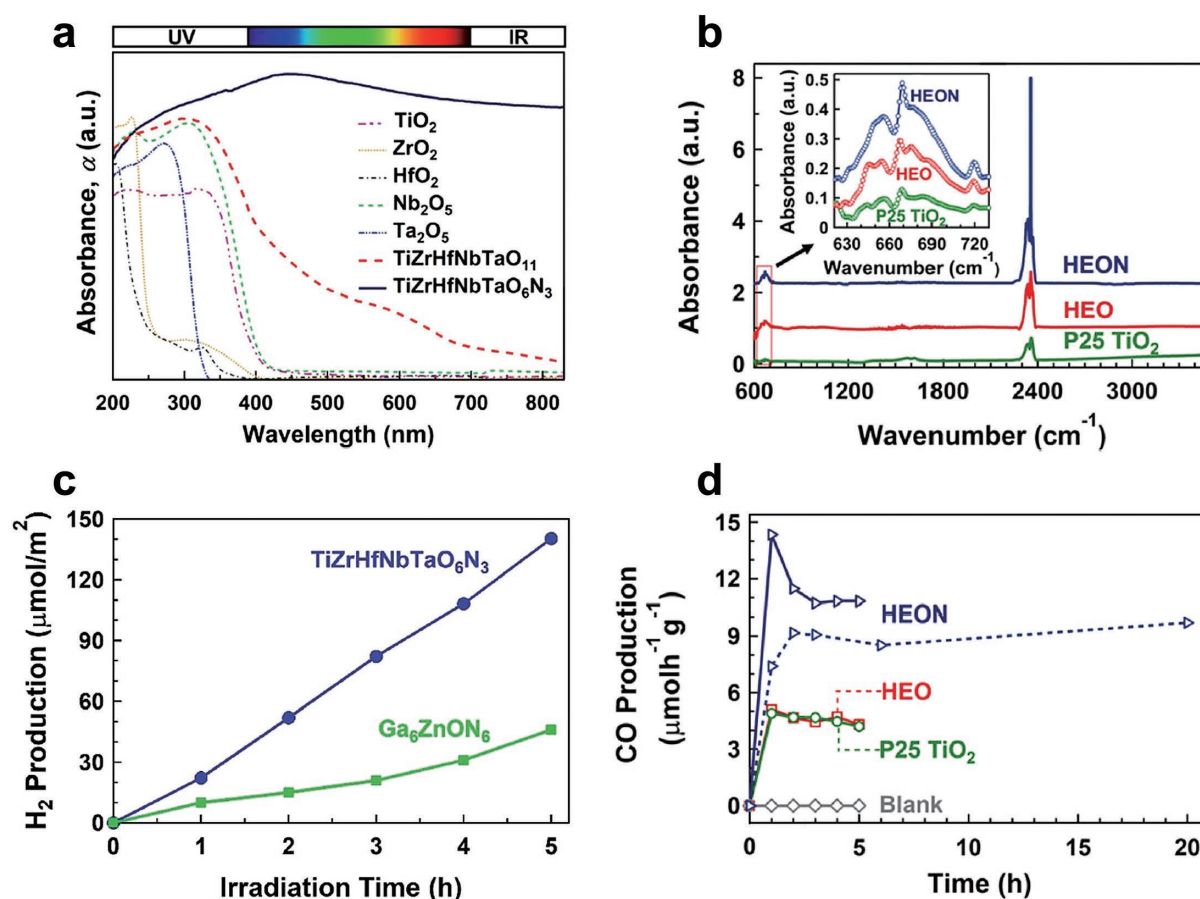


Fig. 7 High light absorbance and significant photocatalytic activity of high-entropy ceramics. (a) UV-vis spectra of TiZrHfNbTaO₁₁, TiZrHfNbTaO₆N₃ and relevant binary oxides including TiO₂, ZrO₂, HfO₂, Nb₂O₅ and Ta₂O₅ (Edalati et al., 2021), (b) diffuse reflectance infrared Fourier transform spectra for TiZrHfNbTaO₁₁ and TiZrHfNbTaO₆N₃ compared with P25 TiO₂ in which the peaks at 665 cm⁻¹ and 2350 cm⁻¹ represent chemisorption and physisorption of CO₂ on surface (Akrami et al., 2022a), (c) photocatalytic hydrogen production on TiZrHfNbTaO₆N₃ compared with Ga₆ZnON₆ (Edalati et al., 2021), and (d) photocatalytic CO₂ to CO conversion on TiZrHfNbTaO₁₁ and TiZrHfNbTaO₆N₃ compared with P25 TiO₂ (Akrami et al., 2022a). Copyright: (2021) Royal Society of Chemistry, (2022) Elsevier.

TiZrHfNbTaO₁₁: TiZrHfNbTaO₁₁ high-entropy oxide (HEO) with two monoclinic and orthorhombic phases which was synthesized by the HPT method and high-temperature oxidation, showed better light absorbance compared to relevant binary oxides including TiO₂, ZrO₂, HfO₂, Nb₂O₅ and Ta₂O₅ (Fig. 7(a)) (Edalati et al., 2020c). This material contained defects such as oxygen vacancies and dislocations as shown in Fig. 8(a). Furthermore, it demonstrated lower photoluminescence intensity compared to anatase TiO₂ and BiVO₄ as two typical photocatalysts, indicating the low recombination rate of electrons and holes in this HEO (Akrami et al., 2022b). Moreover, this material showed the potential to generate photocurrent, produce hydrogen and convert CO₂ to CO under UV light. The rate of hydrogen and CO production for TiZrHfNbTaO₁₁ was higher than anatase TiO₂ and BiVO₄ and almost the same as P25 TiO₂ as a benchmark photocatalyst. This high photocatalytic activity was attributed to the formation of defects, interphases and high-entropy phases which led to the acceleration of electron-hole separation and diminishing their recombination.

TiZrHfNbTaO₆N₃: Low-bandgap high-entropy oxynitride (HEON) TiZrHfNbTaO₆N₃ was produced by HPT processing followed by oxidation and nitriding (Edalati et al., 2021). This HEON showed significantly higher light absorbance compared to corresponding high-entropy and binary oxides (Fig. 7(a)) with a narrow bandgap of 1.6 eV, which is lower than the bandgap of most reported oxynitride photocatalysts in the literature. This HEON could successfully generate photocurrent with a significantly low recombination rate of electrons and holes compared to HEO and P25 TiO₂ as a benchmark photocatalyst (Akrami et al., 2022a). Furthermore, it showed a high potential to adsorb the CO₂ molecules on the surface as shown in Fig. 7(b). This material produced hydrogen under UV irradiation with better activity than Ga₆ZnON₆ as one of the most popular oxynitride photocatalysts (Fig. 7(c)). It also showed a higher photocatalytic activity per surface area for CO₂ conversion compared to HEO and P25 TiO₂ (Fig. 7(d)) and all reported photocatalysts in the literature. Improved photocatalytic activity on this HEON was attributed to the high light absorbance

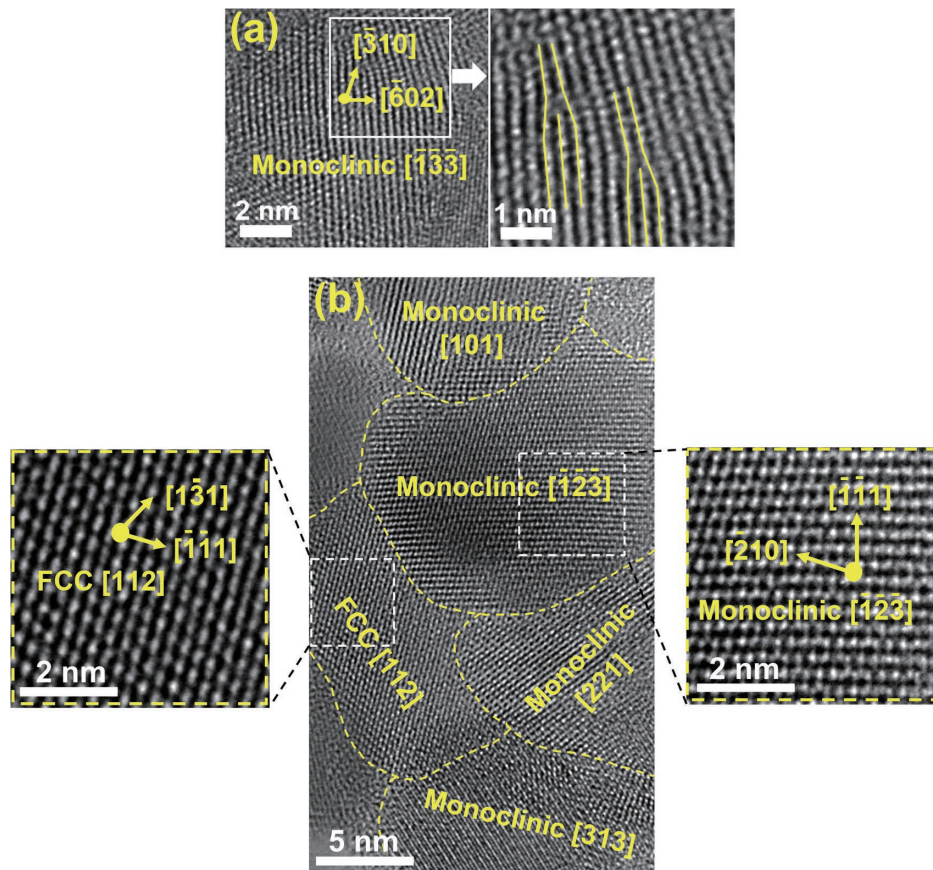


Fig. 8 Formation of nanograins, grain boundaries, interphases, and dislocation defects in high-entropy ceramics synthesized by HPT. High-resolution lattice images of (a) TiZrHfNbTaO_{11} including dislocations (Akrami et al., 2022b) and (b) $\text{TiZrHfNbTaO}_6\text{N}_3$ including monoclinic and FCC phases and their heterojunctions (Edalati et al., 2021). Copyright: (2022) Elsevier, (2021) Royal Society of Chemistry.

and easy electron-hole separation, low recombination rate, and high surface activity for adsorption and conversion of water and CO_2 . The presence of two phases in this HEON and the formation of interphases, as shown in Fig. 8(b), was also believed to contribute to its high activity.

TiZrNbTaWO_{12} : The HEO, TiZrNbTaWO_{12} , was produced by HPT and consequent high-temperature oxidation (Edalati et al., 2022b). It had five different phases including one orthorhombic, two monoclinic and two tetragonal phases and ten heterojunctions. This material showed a low bandgap of 2.3–2.8 eV and a light absorbance higher than relevant binary oxides. Introducing the heterojunctions in this material resulted in successful photocatalytic oxygen production under viable light irradiation.

5. Concluding remark and outlook

Photocatalytic production of hydrogen from water, conversion of CO_2 to value-added compounds and degradation of toxic materials in wastewater under sunlight, are clean processes that have high potential to be used instead of conventional chemical methods. Photocatalysts used for these applications should have a narrow bandgap, appropriate band positions to support

the reactions, low recombination rate of electrons and holes and high surface activity. In recent years, the high-pressure torsion (HPT) method was used to generate active photocatalysts for various applications. This method applies very high strain and pressure to material and subsequently introduces nanocrystals, lattice defects, lattice strain and heterojunctions. Furthermore, HPT can synthesize high-pressure and high-entropy phases. One main reason for the successful application of HPT to develop highly active photocatalysts is that the method can simultaneously introduce a few structural/microstructural features as effective strategies to enhance the activity. It was shown that the HPT method improves photocatalytic activity by increasing light absorbance, decreasing the optical bandgap, optimizing the electronic band structure, accelerating the electron-hole separation and migration and reducing the recombination rate of electrons and holes. The HPT method also contributed to the introduction of high-entropy photocatalysts which show high activity for hydrogen production, oxygen evolution and CO_2 conversion.

Despite the high activity of HPT-processed photocatalysts, the mechanism for their high efficiency needs to be investigated further by employing theoretical calculations.

Moreover, the catalysts produced by HPT have usually low surface area and new methods are expected to be developed to enhance the surface area of these catalysts. Although the HPT method has opened a new path to employing high-pressure and high-entropy phases as new photocatalysts, other synthesis methods should be used in the future for the large-scale production of these new catalysts. It is expected that HPT will continue its contribution to the field of photocatalysis, particularly due to the significance of establishing a carbon-neutral society in recent years.

Acknowledgments

The authors S.A. and P.E. thank Hosokawa Powder Technology Foundation, Japan for funding HPTF21511 and HPTF21512. The author K.E. was supported in part by the MEXT, Japan through Grants-in-Aid for Scientific Research (JP19H05176 & JP21H00150, JP22K18737).

References

- Ajmal A., Majeed I., Malik R.N., Idriss H., Nadeem M.A., Principles and mechanisms of photocatalytic dye degradation on TiO₂ based photocatalysts: a comparative overview, *RSC Advances*, 4 (2014) 37003–37026. DOI: 10.1039/C4RA06658H
- Akpan U.G., Hameed B.H., Parameters affecting the photocatalytic degradation of dyes using TiO₂-based photocatalysts: a review, *Journal of Hazardous Materials*, 170 (2009) 520–529. DOI: 10.1016/j.jhazmat.2009.05.039
- Akrami S., Edalati P., Edalati K., Fuji M., High-entropy ceramics: review of principles, production and applications, *Materials Science and Engineering: R: Reports*, 146 (2021a) 100644. DOI: 10.1016/j.mser.2021.100644
- Akrami S., Edalati P., Shundo Y., Watanabe M., Ishihara T., Fuji M., Edalati K., Significant CO₂ photoreduction on a high-entropy oxynitride, *Chemical Engineering Journal*, 449 (2022a) 137800. DOI: 10.1016/j.cej.2022.137800
- Akrami S., Murakami Y., Watanabe M., Ishihara T., Arita M., Fuji M., Edalati K., Defective high-entropy oxide photocatalyst with high activity for CO₂ conversion, *Applied Catalysis B: Environmental*, 303 (2022b) 120896. DOI: 10.1016/j.apcatb.2021.120896
- Akrami S., Murakami Y., Watanabe M., Ishihara T., Arita M., Guo Q., Fuji M., Edalati K., Enhanced CO₂ conversion on highly-strained and oxygen-deficient BiVO₄ photocatalyst, *Chemical Engineering Journal*, 442 (2022c) 136209. DOI: 10.1016/j.cej.2022.136209
- Akrami S., Watanabe M., Ling T.H., Ishihara T., Arita M., Fuji M., Edalati K., High pressure TiO₂-II polymorph as an active photocatalyst for CO₂ to CO conversion, *Applied Catalysis B: Environmental*, 298 (2021b) 120566. DOI: 10.1016/j.apcatb.2021.120566
- Albedwawi S.H., AlJaberi A., Haidemenopoulos G.N., Polychronopoulos K., High entropy oxides-exploring a paradigm of promising catalysts: a review, *Materials & Design*, 202 (2021) 109534. DOI: 10.1016/j.matdes.2021.109534
- Bérardan D., Franger S., Dragoë D., Meena A.K., Dragoë N., Colossal dielectric constant in high entropy oxides, *Physica Status Solidi (RRL)—Rapid Research Letters*, 10 (2016) 328–333. DOI: 10.1002/pssr.201600043
- Bridgman P.W., Effects of high shearing stress combined with high hydrostatic pressure, *Physical Review*, 48 (1935) 825–847. DOI: 10.1103/PhysRev.48.825
- Cao S., Shen B., Tong T., Fu J., Yu J., 2D/2D heterojunction of ultrathin MXene/Bi₂WO₆ nanosheets for improved photocatalytic CO₂ reduction, *Advanced Functional Materials*, 28 (2018) 1800136. DOI: 10.1002/adfm.201800136
- Chakrabarti S., Dutta B.K., Photocatalytic degradation of model textile dyes in wastewater using ZnO as semiconductor catalyst, *Journal of Hazardous Materials*, 112 (2004) 269–278. DOI: 10.1016/j.jhazmat.2004.05.013
- Delogu F., Are processing conditions similar in ball milling and high-pressure torsion? The case of the tetragonal-to-monoclinic phase transition in ZrO₂ powders, *Scripta Materialia*, 67 (2012) 340–343. DOI: 10.1016/j.scriptamat.2012.05.031
- Di J., Song P., Zhu C., Chen C., Xiong J., Duan M., Long R., Zhou W., Xu M., Kang L., Lin Bo, Liu D., Chen S., Liu C., Li H., Zhao Y., Li S., Yan Q., Song L., Liu Z., Strain-engineering of Bi₁₂O₁₇Br₂ nanotubes for boosting photocatalytic CO₂ reduction, *ACS Materials Letter*, 2 (2020) 1025–1032. DOI: 10.1021/acsmaterialslett.0c00306
- Edalati K., Metallurgical alchemy by ultra-severe plastic deformation via high-pressure torsion process, *Materials Transactions*, 60 (2019a) 1221–1229. DOI: 10.2320/matertrans.MF201914
- Edalati K., Review on recent advancements in severe plastic deformation of oxides by high-pressure torsion (HPT), *Advanced Engineering Materials*, 21 (2019b) 1800272. DOI: 10.1002/adem.201800272
- Edalati K., Arimura M., Ikoma Y., Daio T., Miyata T., Smith D.J., Horita Z., Plastic deformation of BaTiO₃ ceramics by high-pressure torsion and changes in phase transformations, optical and dielectric properties, *Materials Research Letters*, 3 (2015a) 216–221. DOI: 10.1080/21663831.2015.1065454
- Edalati K., Bachmaier A., Beloshenko V.A., Beygelzimer Y., Blank V.D., Botta W.J., Bryla K., Čížek J., Divinski S., Enikeev N.A., Estrin Y., Faraji G., Figueiredo R.B., Fuji M., Furuta T., et al., Nanomaterials by severe plastic deformation: review of historical developments and recent advances, *Materials Research Letters*, 10 (2022a) 163–256. DOI: 10.1080/21663831.2022.2029779
- Edalati K., Emami H., Staykov A., Smith D.J., Akiba E., Horita Z., Formation of metastable phases in magnesium-titanium system by high-pressure torsion and their hydrogen storage performance, *Acta Materialia*, 99 (2015b) 150–156. DOI: 10.1016/j.actamat.2015.07.060
- Edalati K., Fujita I., Sauvage X., Arita M., Horita Z., Microstructure and phase transformations of silica glass and vanadium oxide by severe plastic deformation via high-pressure torsion straining, *Journal of Alloys and Compounds*, 779 (2019a) 394–398. DOI: 10.1016/j.jallcom.2018.11.086
- Edalati K., Fujita I., Takechi S., Nakashima Y., Kumano K., Razavi-Khosroshahi H., Arita M., Watanabe M., Sauvage X., Akbay T., Ishihara T., Fuji M., Horita Z., Photocatalytic activity of aluminum oxide by oxygen vacancy generation using high-pressure torsion straining, *Scripta Materialia*, 173 (2019b) 120–124. DOI: 10.1016/j.scriptamat.2019.08.011
- Edalati K., Fujiwara K., Takechi S., Wang Q., Arita M., Watanabe M., Sauvage X., Ishihara T., Horita Z., Improved photocatalytic hydrogen evolution on tantalate perovskites CsTaO₃ and LiTaO₃ by strain-induced vacancies, *ACS Applied Energy Materials*, 3 (2020a) 1710–1718. DOI: 10.1021/acsaem.9b02197
- Edalati K., Horita Z., Scaling-up of high-pressure torsion using ring shape, *Materials Transactions*, 50 (2009) 92–95. DOI: 10.2320/matertrans.MD200822
- Edalati K., Horita Z., Application of high-pressure torsion for consolidation of ceramic Powders, *Scripta Materialia*, 63 (2010) 174–177. DOI: 10.1016/j.scriptamat.2010.03.048
- Edalati K., Horita Z., Mine Y., High-pressure torsion of hafnium, *Materials Science and Engineering: A*, 527 (2010a) 2136–2141. DOI: 10.1016/j.msea.2009.11.060
- Edalati K., Horita Z., High-pressure torsion of pure metals: Influence of atomic bond parameters and stacking fault energy on grain size and correlation with hardness, *Acta Materialia*, 59 (2011) 6831–6836. DOI: 10.1016/j.actamat.2011.07.046

- Edalati K., Horita Z., A review on high-pressure torsion (HPT) from 1935 to 1988, *Materials Science and Engineering: A*, 652 (2016) 325–352. DOI: 10.1016/j.msea.2015.11.074
- Edalati K., Toh S., Ikoma Y., Horita Z., Plastic deformation and allotropic phase transformations in zirconia ceramics during high-pressure torsion, *Scripta Materialia*, 65 (2011) 974–977. DOI: 10.1016/J.SCRIPTAMAT.2011.08.024
- Edalati K., Uehiro R., Takechi S., Wang Q., Arita M., Watanabe M., Ishihara T., Horita Z., Enhanced photocatalytic hydrogen production on GaN-ZnO oxynitride by introduction of strain-induced nitrogen vacancy complexes, *Acta Materialia*, 185 (2020b) 149–156. DOI: 10.1016/j.actamat.2019.12.007
- Edalati K., Wang Q., Eguchi H., Razavi-Khosroshahi H., Emami H., Yamauchi M., Fuji M., Horita Z., Impact of TiO₂-II phase stabilized in anatase matrix by high-pressure torsion on electrocatalytic hydrogen production, *Materials Research Letters*, 7 (2019c) 334–339. DOI: 10.1080/21663831.2019.1609111
- Edalati K., Wang Q., Razavi-Khosroshahi H., Emami H., Fuji M., Horita Z., Low-temperature anatase-to-rutile phase transformation and unusual grain coarsening in titanium oxide nanopowders by high-pressure torsion straining, *Scripta Materialia*, 162 (2019d) 341–344. DOI: 10.1016/j.scriptamat.2018.11.044
- Edalati K., Yokoyama Y., Horita Z., High-pressure torsion of machining chips and bulk discs of amorphous Zr₅₀Cu₃₀Al₁₀Ni₁₀, *Materials Transactions*, 51 (2010b) 23–26. DOI: 10.2320/matertrans.MB200914
- Edalati P., Itagoe Y., Ishihara H., Ishihara T., Emami H., Arita M., Fuji M., Edalati K., Visible-light photocatalytic oxygen production on a high-entropy oxide by multiple-heterojunction introduction, *Journal of Photochemistry and Photobiology A: Chemistry*, 433 (2022b) 114167. DOI: 10.1016/j.jphotochem.2022.114167
- Edalati P., Shen X.F., Watanabe M., Ishihara T., Arita M., Fuji M., Edalati K., High-entropy oxynitride as a low-bandgap and stable photocatalyst for hydrogen production, *Journal of Materials Chemistry A*, 9 (2021) 15076–15086. DOI: 10.1039/D1TA03861C
- Edalati P., Wang Q., Razavi-Khosroshahi H., Fuji M., Ishihara T., Edalati K., Photocatalytic hydrogen evolution on a high entropy oxide, *Journal of Materials Chemistry A*, 8 (2020c) 3814–3821. DOI: 10.1039/C9TA12846H
- Estrin Y., Vinogradov A., Extreme grain refinement by severe plastic deformation: a wealth of challenging science, *Acta Materialia*, 61 (2013) 782–817. DOI: 10.1016/j.actamat.2012.10.038
- Etman A.S., Abdelhamid H.N., Yuan Y., Wang L., Zou X., Sun J., Facile water-based strategy for synthesizing MoO_{3-x} nanosheets: efficient visible light photocatalysts for dye degradation, *ACS Omega*, 3 (2018) 2193–2201. DOI: 10.1021/acsomega.8b00012
- Feng B., Levitas V.I., Coupled elastoplasticity and plastic strain-induced phase transformation under high pressure and large strains: formulation and application to BN sample compressed in a diamond anvil cell, *International Journal of Plasticity*, 96 (2017) 156–181. DOI: 10.1016/j.ijplas.2017.05.002
- Feng B., Levitas V.I., Li W., FEM modeling of plastic flow and strain-induced phase transformation in BN under high pressure and large shear in a rotational diamond anvil cell, *International Journal of Plasticity*, 113 (2019) 236–254. DOI: 10.1016/j.ijplas.2018.10.004
- Feng H., Xu Z., Wang L., Yu Y., Mitchell D., Cui D., Xu X., Shi J., Sannomiya T., Du Y., Hao W., Dou S.X., Modulation of photocatalytic properties by strain in 2D BiOBr nanosheets, *ACS Applied Materials & Interfaces*, 7 (2015) 27592–27596. DOI: 10.1021/acsami.5b08904
- Fu J., Jiang K., Qiu X., Yu J., Liu M., Product selectivity of photocatalytic CO₂ reduction reactions, *Materials Today*, 32 (2020) 222–243. DOI: 10.1016/j.mattod.2019.06.009
- Fujita I., Edalati K., Wang Q., Arita M., Watanabe M., Munetoh S., Ishihara T., Horita Z., High-pressure torsion to induce oxygen vacancies in nanocrystals of magnesium oxide: enhanced light absorbance, photocatalysis and significance in geology, *Materialia*, 11 (2020a) 100670. DOI: 10.1016/j.mtla.2020.100670
- Fujita I., Edalati P., Wang Q., Watanabe M., Arita M., Munetoh S., Ishihara T., Edalati K., Novel black bismuth oxide (Bi₂O₃) with enhanced photocurrent generation, produced by high-pressure torsion straining, *Scripta Materialia*, 187 (2020b) 366–370. DOI: 10.1016/j.scriptamat.2020.06.052
- Gao S., Gu B., Jiao X., Sun Y., Zu X., Yang F., Zhu W., Wang C., Feng Z., Ye B., Xie Y., Highly efficient and exceptionally durable CO₂ photoreduction to methanol over freestanding defective single-unit-cell bismuth vanadate layers, *Journal of the American Chemical Society*, 139 (2017) 3438–3445. DOI: 10.1021/jacs.6b11263
- Gaya U.I., Abdullah A.H., Heterogeneous photocatalytic degradation of organic contaminants over titanium dioxide: a review of fundamentals, progress and problems, *Journal of Photochemistry and Photobiology C: Photochemistry Reviews*, 9 (2008) 1–12. DOI: 10.1016/j.jphotochemrev.2007.12.003
- Gizhevskii B.A., Sukhorukov Y.P., Nomerovannaya L.V., Makhnev A.A., Ponosov Y.S., Telegin A.V., Mostovshchikov E.V., Features of optical properties and the electronic structure of nanostructured oxides of 3d-Metals, *Solid State Phenomenon*, 168-169 (2011) 317–320. DOI: 10.4028/www.scientific.net/SSP.168-169.317
- Habisreutinger A.S.N., Schmidt-Mende L., Stolarczyk J.K., Photocatalytic reduction of CO₂ on TiO₂ and other semiconductors, *Angewandte Chemie International Edition*, 52 (2013) 7372–7408. DOI: 10.1002/anie.201207199
- Hagiwara H., Kakigi R., Takechi S., Watanabe M., Hinokuma S., Ida S., Ishihara T., Effects of preparation condition on the photocatalytic activity of porphyrin-modified GaN:ZnO for water splitting, *Surface and Coatings Technology*, 324 (2017) 601–606. DOI: 10.1016/j.surfcoat.2016.10.054
- Hidalgo-Jimenez J., Wang Q., Edalati K., Cubero-Sesin J.M., Razavi-Khosroshahi H., Ikoma Y., Gutiérrez-Fallas D., Dittel-Meza F.A., Rodríguez-Rufino J.C., Fuji M., Horita Z., Phase transformations, vacancy formation and variations of optical and photocatalytic properties in TiO₂-ZnO composites by high-pressure torsion, *International Journal of Plasticity*, 124 (2020) 170–185. DOI: 10.1016/j.ijplas.2019.08.010
- Huang S.T., Lee W.W., Chang J.L., Huang W.S., Cho S.Y., Chen C.C., Hydrothermal synthesis of SrTiO₃ nanocubes: characterization, photocatalytic activities, and degradation pathway, *Journal of the Taiwan Institute of Chemical Engineers*, 45 (2014a) 1927–1936. DOI: 10.1016/j.jtice.2014.02.003
- Huang Y., Li H., Balogun M.S., Liu W., Tong Y., Lu X., Ji H., Oxygen vacancy induced bismuth oxyiodide with remarkably increased visible-light absorption and superior photocatalytic performance, *ACS Applied Materials & Interfaces*, 6 (2014b) 22920–22927. DOI: 10.1021/am507641k
- Ikoma Y., Hayano K., Edalati K., Saito K., Guo Q., Horita Z., Phase transformation and nanograin refinement of silicon by processing through high-pressure torsion, *Applied Physics Letters*, 101 (2012) 121908. DOI: 10.1063/1.4754574
- Iwashina K., Kudo A., Rh-Doped SrTiO₃ photocatalyst electrode showing cathodic photocurrent for water splitting under visible-light irradiation, *Journal of the American Chemical Society*, 133 (2011) 13272–13275. DOI: 10.1021/ja2050315
- Jin T., Sang X., Unocic R.R., Kinch R.T., Liu X., Hu J., Liu H., Dai S., Mechanochemical assisted synthesis of high-entropy metal nitride via a soft urea strategy, *Advanced Materials*, 30 (2018) 1707512. DOI: 10.1002/adma.201707512
- Kuvarega A.T., Krause R.W.M., Mamba B.B., Nitrogen/palladium-codoped TiO₂ for efficient visible light photocatalytic dye degradation, *The Journal of Physical Chemistry C*, 115 (2011) 22110–22120. DOI: 10.1021/jp203754j

- Kuznetsova E.I., Degtyarev M.V., Zyuzeva, I.B. Bobylev N.A., Pilyugin V.P., Microstructure of $\text{YBa}_2\text{Cu}_3\text{O}_y$ subjected to severe plastic deformation by high pressure torsion, *Physics of Metals and Metallography*, 118 (2017) 773–781. DOI: 10.1134/S0031918X17080099
- Lee G.J., Anandan S., Masten S.J., Wu J.J., Photocatalytic hydrogen evolution from water splitting using Cu doped ZnS microspheres under visible light irradiation, *Renewable Energy*, 89 (2016) 18–26. DOI: 10.1016/j.renene.2015.11.083
- Lei F., Sun Y., Liu K., Gao S., Liang L., Pan B., Xie Y., Oxygen vacancies confined in ultrathin indium oxide porous sheets for promoted visible-light water splitting, *Journal of the American Chemical Society*, 136 (2014) 6826–6829. DOI: 10.1021/ja501866r
- Li F., Zhou L., Liu J.X., Liang Y., Zhang G.J., High-entropy pyrochlores with low thermal conductivity for thermal barrier coating materials, *Journal of Advanced Ceramics*, 8 (2019) 576–582. DOI: 10.1007/s40145-019-0342-4
- Li X., Xie J., Jiang C., Yu J., Zhang P., Review on design and evaluation of environmental Photocatalysts, *Frontiers of Environmental Science & Engineering*, 12 (2018) 14. DOI: 10.1007/s11783-018-1076-1
- Li Y., Wang W.N., Zhan Z., Woo M.H., Wu C.Y., Biswas P., Photocatalytic reduction of CO_2 with H_2O on mesoporous silica supported Cu/TiO₂ catalysts, *Applied Catalysis B: Environmental*, 100 (2010) 386–392. DOI: 10.1016/j.apcatb.2010.08.015
- Liang B., Ai Y., Wang Y., Liu C., Ouyang S., Liu M., Spinel-type $(\text{FeCoCrMnZn})_3\text{O}_4$ high-entropy oxide: facile preparation and supercapacitor performance, *Materials*, 13 (2020) 5798. DOI: 10.3390/ma13245798
- Lin Y.G., Hsu Y.K., Chen Y.C., Chen L.C., Chen S.Y., Chen K.H., Visible-light-driven photocatalytic carbon-doped porous ZnO nanoarchitectures for solar water-splitting, *Nanoscale*, 4 (2012) 6515–6519. DOI: 10.1039/C2NR31800H
- Liu B., Ye L., Wang R., Yang J., Zhang Y., Guan R., Tian L., Chen X., Phosphorus-doped graphitic carbon nitride nanotubes with amino-rich surface for efficient CO_2 capture, enhanced photocatalytic activity, and product selectivity, *ACS Applied Materials & Interfaces*, 10 (2018) 4001–4009. DOI: 10.1021/acsami.7b17503
- Liu Y., Ohko Y., Zhang R., Yang Y., Zhang Z., Degradation of malachite green on Pd/WO₃ photocatalysts under simulated solar light, *Journal of Hazardous Materials*, 184 (2010) 386–391. DOI: 10.1016/j.jhazmat.2010.08.047
- Lu H., Tournet J., Dastafkan K., Liu Y., Ng Y.H., Karuturi S.K., Zhao C., Yin Z., Noble-metal-free multicomponent nanointegration for sustainable energy conversion, *Chemical Reviews*, 121 (2021) 10271–10366. DOI: 10.1021/acs.chemrev.0c01328
- Lun Z., Ouyang B., Kwon D.H., Ha Y., Foley E.E., Huang T.Y., Cai Z., Kim H., Balasubramanian M., Sun Y., Huang J., Tian Y., Kim H., McCloskey B.D., Yang W., Clément R.J., Ji H., Ceder G., Cation-disordered rocksalt-type high-entropy cathodes for Li-ion batteries, *Nature Materials*, 20 (2021) 214–221. DOI: 10.1038/s41563-020-00816-0
- Ma Y., Wang X., Jia Y., Chen X., Han H., Li C., Titanium dioxide-based nanomaterials for photocatalytic fuel, *Chemical Reviews*, 114 (2014) 9987–10043. DOI: 10.1021/cr500008u.
- Maeda K., Photocatalytic water splitting using semiconductor particles: history and recent developments, *Journal of Photochemistry and Photobiology C: Photochemistry Reviews*, 12 (2011) 237–268. DOI: 10.1016/j.jphotochemrev.2011.07.001
- Maeda K., Domen K., New non-oxide photocatalysts designed for overall water splitting under visible light, *The Journal of Physical Chemistry C*, 111 (2007) 7851–7861. DOI: 10.1021/jp070911w
- Maeda K., Takata T., Hara M., Saito N., Inoue Y., Kobayashi H., Domen K., GaN:ZnO Solid solution as a photocatalyst for visible-light-driven overall water splitting, *Journal of the American Chemical Society*, 127 (2005) 8286–8287. DOI: 10.1021/ja0518777
- Makhnev A.A., Nomerovannaya L.V., Gizhevskii B.A., Naumov S.V., Kostromitin N.V., Effect of redistribution of the optical spectral weight in CuO nanostructured ceramics, *Solid State Phenomenon*, 168-169 (2011) 285–288. DOI: 10.4028/www.scientific.net/SSP.168-169.285
- Moniz S.J.A., Shevlin S.A., Martin D.J., Guo Z.X., Tang J., Visible-light driven heterojunction photocatalysts for water splitting — a critical review, *Energy & Environmental Science*, 8 (2015) 731–759. DOI: 10.1039/C4EE03271C
- Mostovshchikova E.V., Gizhevskii B.A., Loshkareva N.N., Galakhov V.R., Naumov S.V., Ponomov Y.S., Ovechkina N.A., Kostromitina N.V., Buling A., Neumann M., Infrared and X-ray absorption spectra of Cu₂O and CuO nanoceramics, *Solid State Phenomenon*, 190 (2012) 683–686. DOI: 10.4028/www.scientific.net/SSP.190.683
- Nguyen T.X., Patra J., Chang J.K., Ting J.M., High entropy spinel oxide nanoparticles for superior lithiation–delithiation performance, *Journal of Materials Chemistry A*, 8 (2020) 18963–18973. DOI: 10.1039/D0TA04844E
- Ni M., Leung M.K.H., Leung D.Y.C., Sumathy K., A review and recent developments in photocatalytic water-splitting using TiO₂ for hydrogen production, *Renewable and Sustainable Energy Reviews*, 11 (2007) 401–425. DOI: 10.1016/j.rser.2005.01.009
- Ohno T., Bai L., Hisatomi T., Maeda K., Domen K., Photocatalytic water splitting using modified GaN:ZnO solid solution under visible light: long-time operation and regeneration of activity, *Journal of the American Chemical Society*, 134 (2012) 8254–8259. DOI: 10.1021/ja302479f
- Ola O., Maroto-Valer M.M., Review of material design and reactor engineering on TiO₂ photocatalysis for CO₂ reduction, *Journal of Photochemistry and Photobiology C: Photochemistry Reviews*, 24 (2015) 16–42. DOI: 10.1016/j.jphotochemrev.2015.06.001
- Oses C., Toher C., Curtarolo S., High-entropy ceramics, *Nature Reviews Materials*, 5 (2020) 295–309. DOI: 10.1038/s41578-019-0170-8
- Pauptert T., Rathouský J., Electrodeposited mesoporous ZnO thin films as efficient photocatalysts for the degradation of dye pollutants, *Journal of Physical Chemistry C*, 111 (2007) 7639–7644. DOI: 10.1021/jp071465f
- Permyakova I., Glezer A., Amorphous-nanocrystalline composites prepared by high-pressure torsion, *Metals*, 10 (2020) 511. DOI: 10.3390/met10040511
- Puangpett T., Sreethawong T., Yoshikawa S., Chavadej S., Hydrogen production from photocatalytic water splitting over mesoporous-assembled SrTiO₃ nanocrystal-based photocatalysts, *Journal of Molecular Catalysis A: Chemical*, 312 (2009) 97–106. DOI: 10.1016/j.molcata.2009.07.012
- Qi Y., Kauffmann Y., Kosinova A., Kilmametov A.R., Straumal B.B., Rabkin E., Gradient bandgap narrowing in severely deformed ZnO nanoparticles, *Materials Research Letters*, 9 (2021) 58–64. DOI: 10.1080/21663831.2020.1821111
- Qi Y., Kosinova A., Kilmametov A.R., Straumal B.B., Rabkin E., Plastic flow and microstructural instabilities during high-pressure torsion of Cu/ZnO composites, *Materials Characterization*, 145 (2018) 389–401. DOI: 10.1016/j.matchar.2018.09.001
- Qian C., He Z., Liang C., Ji W., New in situ synthesis method for Fe₃O₄/flake graphite nanosheet composite structure and its application in anode materials of lithium-ion batteries, *Journal of Nanomaterials*, 2018 (2018) 2417949. DOI: 10.1155/2018/2417949
- Qiao H., Wang X., Dong Q., Zheng H., Chen G., Hong M., Yang C.P., Wu M., He K., Hu L., A high-entropy phosphate catalyst for oxygen evolution reaction, *Nano Energy*, 86 (2021) 106029. DOI: 10.1016/j.nanoen.2021.106029
- Razavi-Khosroshahi H., Edalati K., Arita M., Horita Z., Fuji M., Plastic strain and grain size effect on high-pressure phase transformations in nanostructured TiO₂ ceramics, *Scripta Materialia*, 124 (2016a) 59–62. DOI: 10.1016/j.scriptamat.2016.06.022
- Razavi-Khosroshahi H., Edalati K., Emami H., Akiba E., Horita Z., Fuji

- M., Optical properties of nanocrystalline monoclinic Y_2O_3 stabilized by grain size and plastic strain effects via high-pressure torsion, *Inorganic Chemistry*, 56 (2017a) 2576–2580. DOI: 10.1021/acs.inorgchem.6b02725
- Razavi-Khosroshahi H., Edalati K., Hirayama M., Emami H., Arita M., Yamauchi M., Hagiwara H., Ida S., Ishihara T., Akiba E., Horita Z., Fuji M., Visible-light-driven photocatalytic hydrogen generation on nanosized TiO_2 -II stabilized by high-pressure torsion, *ACS Catalysis*, 6 (2016b) 5103–5107. DOI: 10.1021/acscatal.6b01482
- Razavi-Khosroshahi H., Edalati K., Wu J., Nakashima Y., Arita M., Ikoma Y., Sadakiyo M., Inagaki Y., Staykov A., Yamauchi M., Horita Z., Fuji M., High-pressure zinc oxide phase as visible-light-active photocatalyst with narrow band gap, *Journal of Materials Chemistry A*, 5 (2017b) 20298–20303. DOI: 10.1039/C7TA05262F
- Ren K., Wang Q., Shao G., Zhao X., Wang Y., Multicomponent high-entropy zirconates with comprehensive properties for advanced thermal barrier coating, *Scripta Materialia*, 178 (2020) 382–386. DOI: 10.1016/j.scriptamat.2019.12.006
- Sa B., Li Y.-L., Qi J., Ahuja R., Sun Z., Strain engineering for phosphorene: the potential application as a photocatalyst, *The Journal of Physical Chemistry C*, 118 (2014) 26560–26568. DOI: 10.1021/jp508618t
- Shabashov V.A., Makarov A.V., Kozlov K.A., Sagaradze V.V., Zamatovskii A.E., Volkova E.G., Luchko S.N., Deformation-induced dissolution and precipitation of nitrides in austenite and ferrite of a high-nitrogen stainless steel, *Physics of Metals and Metallography*, 119 (2018) 180–190. DOI: 10.1134/S0031918X18020096
- Shan J., Raziq F., Humayun M., Zhou W., Qu Y., Wang G., Li Y., Improved charge separation and surface activation via boron-doped layered polyhedron SrTiO_3 for co-catalyst free photocatalytic CO_2 conversion, *Applied Catalysis B: Environmental*, 219 (2017) 10–17. DOI: 10.1016/j.apcatb.2017.07.024
- Starink M.J., Cheng X., Yang S., Hardening of pure metals by high-pressure torsion: A physically based model employing volume-averaged defect evolutions, *Acta Materialia*, 61 (2013) 183–192. DOI: 10.1016/j.actamat.2012.09.048
- Sun S., Wang W., Li D., Zhang L., Jiang D., Solar light driven pure water splitting on quantum sized BiVO_4 without any cocatalyst, *ACS Catalysis*, 4 (2014) 3498–3503. DOI: 10.1021/cs501076a
- Talluri B., Aparna M.L., Sreenivasulu N., Bhattacharya S.S., Thomas T., High entropy spinel metal oxide $(\text{CoCrFeMnNi})_3\text{O}_4$ nanoparticles as a high-performance supercapacitor electrode material, *Journal of Energy Storage*, 42 (2021) 103004. DOI: 10.1016/j.est.2021.103004
- Telegin A.V., Gizhevskii B.A., Nomerovannaya L.V., Makhnev A.A., The optical and magneto-optical properties of nanostructured oxides of 3d-metals, *Journal of Superconductivity and Novel Magnetism*, 25 (2012) 2683–2686. DOI: 10.1007/s10948-011-1242-1
- Tong H., Ouyang S., Bi Y., Umezawa N., Oshikiri M., Ye J., Nano-photocatalytic materials: possibilities and challenges, *Advanced Materials*, 24 (2012) 229–251. DOI: 10.1002/adma.201102752
- Tu W., Zhou Y., Liu Q., Tian Z., Gao J., Chen X., Zhang H., Liu J., Zou Z., Robust hollow spheres consisting of alternating titania nanosheets and graphene nanosheets with high photocatalytic activity for CO_2 conversion into renewable fuels, *Advanced Functional Materials*, 22 (2012) 1215–1221. DOI: 10.1002/adfm.201102566
- Tu W., Zhou Y., Zou Z., Photocatalytic conversion of CO_2 into renewable hydrocarbon fuels: state-of-the-art accomplishment, challenges, and prospects, *Advanced Materials*, 26 (2014) 4607–4626. DOI: 10.1002/adma.201400087
- Uddin M.T., Nicolas Y., Olivier C., Toupance T., Servant L., Müller M.M., Kleebe H.J., Ziegler J., Jaegermann W., Nanostructured SnO_2 -ZnO heterojunction photocatalysts showing enhanced photocatalytic activity for the degradation of organic dyes, *Inorganic Chemistry*, 51 (2012) 7764–7773. DOI: 10.1021/ic300794j
- Valiev R., Nanostructuring of metals by severe plastic deformation for advanced properties, *Nature Materials*, 3 (2004) 511–516. DOI: 10.1038/nmat1180
- Wang F., Valentin C.D., Pacchioni G., Doping of WO_3 for photocatalytic water splitting: hints from density functional theory, *The Journal of Physical Chemistry C*, 116 (2012) 8901–8909. DOI: 10.1021/jp300867j
- Wang H., Zhang L., Wang K., Sun X., Wang W., Enhanced photocatalytic CO_2 reduction to methane over $\text{WO}_3 \cdot 0.33\text{H}_2\text{O}$ via Mo doping, *Applied Catalysis B: Environmental*, 243 (2019a) 771–779. DOI: 10.1016/j.apcatb.2018.11.021
- Wang K., Lu J., Lu Y., Lau C.H., Zheng Y., Fan X., Unravelling the C-C coupling in CO_2 photocatalytic reduction with H_2O on Au/TiO_{2-x} : combination of plasmonic excitation and oxygen vacancy, *Applied Catalysis B: Environmental*, 292 (2021) 120147. DOI: 10.1016/j.apcatb.2021.120147
- Wang Q., Edalati K., Fujita I., Watanabe M., Ishihara T., Horita Z., High-pressure torsion of SiO_2 quartz sand: Phase transformation, optical properties, and significance in geology, *Journal of the American Ceramic Society*, 103 (2020a) 6594–6602. DOI: 10.1111/jace.17362
- Wang Q., Edalati K., Koganemaru Y., Nakamura S., Watanabe M., Ishihara T., Horita Z., Photocatalytic hydrogen generation on low-band-gap black zirconia (ZrO_2) produced by high-pressure torsion, *Journal of Materials Chemistry A*, 8 (2020b) 3643–3650. DOI: 10.1039/C9TA11839J
- Wang Q., Sarkar A., Wang D., Velasco L., Azmi R., Bhattacharya S.S., Bergfeldt T., Düvel A., Heitjans P., Brezesinski T., Hahn H., Breitung B., Multi-anionic and -cationic compounds: new high entropy materials for advanced Li-ion batteries, *Energy & Environmental Science*, 12 (2019b) 2433–2442. DOI: 10.1039/C9EE00368A
- Wang Q., Watanabe M., Edalati K., Visible-light photocurrent in nano-structured high-pressure TiO_2 -II (Columbite) Phase, *The Journal of Physical Chemistry C*, 124 (2020c) 13930–13935. DOI: 10.1021/acs.jpcc.0c03923
- Wen J., Xie J., Chen X., Li X., A review on g- C_3N_4 -based photocatalysts, *Applied Surface Science*, 391 (2017) 72–123. DOI: 10.1016/j.apsusc.2016.07.030
- Xiang H., Xing Y., Dai F., Wang H., Su L., Miao L., Zhang G., Wang Y., Qi X., Yao L., Wang H., Zhao B., Li J., Zhou Y., High-entropy ceramics: present status, challenges, and a look forward, *Journal of Advanced Ceramics*, 10 (2021) 385–441. DOI: 10.1007/s40145-021-0477-y
- Xu H., Zhang Z., Liu J., Do-Thanh C.L., Chen H., Xu S., Lin Q., Jiao Y., Wang J., Wang Y., Chen Y., Dai S., Entropy-stabilized single-atom Pd catalysts via high-entropy fluorite oxide supports, *Nature Communications*, 11 (2020) 3908. DOI: 10.1038/s41467-020-17738-9
- Ye S., Wang R., Wu M.Z., Yuan Y.P., A review on g- C_3N_4 for photocatalytic water splitting and CO_2 reduction, *Applied Surface Science*, 358 (2015) 15–27. DOI: 10.1016/j.apsusc.2015.08.173
- Yu H., Li J., Zhang Y., Yang S., Han K., Dong F., Ma T., Huang H., Three-in-one oxygen vacancies: whole visible-spectrum absorption, efficient charge separation, and surface site activation for robust CO_2 photoreduction, *Angewandte Chemie International Edition*, 58 (2019) 3880–3884. DOI: 10.1002/anie.201813967
- Yu J., Qi L., Jaroniec M., Hydrogen production by photocatalytic water splitting over Pt/TiO_2 nanosheets with exposed (001) facets, *The Journal of Physical Chemistry C*, 114 (2010) 13118–13125. DOI: 10.1021/jp104488b
- Yuan X., Zhou C., Jin Y., Jing Q., Yang Y., Shen X., Tang Q., Mu Y., Du A.K., Facile synthesis of 3D porous thermally exfoliated g- C_3N_4 nanosheet with enhanced photocatalytic degradation of organic dye, *Journal of Colloid and Interface Science*, 468 (2016) 211–219. DOI: 10.1016/j.jcis.2016.01.048
- Zhang D., Yu Y., Feng X., Tian Z., Song R., Thermal barrier coatings with high-entropy oxide as a top coat, *Ceramics International*, 48 (2022) 1349–1359. DOI: 10.1016/j.ceramint.2021.09.219

- Zhang R.Z., Reece M.J., Review of high entropy ceramics: design, synthesis, structure and properties, *Journal of Materials Chemistry A*, 7 (2019) 22148–22162. DOI: 10.1039/C9TA05698J
- Zhao J., Liu B., Meng L., He S., Yuan R., Hou Y., Ding Z., Lin H., Zhang Z., Wang X., Long J., Plasmonic control of solar-driven CO₂ conversion at the metal/ZnO interfaces, *Applied Catalysis B: Environmental*, 256 (2019) 117823. DOI: 10.1016/j.apcatb.2019.117823
- Zhou B., Zhao X., Liu H., Qu J., Huang C.P., Visible-light sensitive cobalt-doped BiVO₄ (Co-BiVO₄) photocatalytic composites for the degradation of methylene blue dye in dilute aqueous solutions, *Applied Catalysis B: Environmental*, 99 (2010) 214–221. DOI:

10.1016/j.apcatb.2010.06.022

- Zhou S., Pu Y., Zhang Q., Shi R., Guo X., Wang W., Ji J., Wei T., Ouyang T., Microstructure and dielectric properties of high entropy Ba (Zr_{0.2}Ti_{0.2}Sn_{0.2}Hf_{0.2}Me_{0.2})O₃ perovskite oxides, *Ceramics International*, 46 (2020) 7430–7437. DOI: 10.1016/j.ceramint.2019.11.239
- Zhou S., Pu Y., Zhao X., Ouyang T., Ji J., Zhang Q., Zhang C., Sun S., Sun R., Li J., Wang D., Dielectric temperature stability and energy storage performance of NBT-based ceramics by introducing high-entropy oxide, *Journal of the American Ceramic Society*, 105 (2022) 4796–4804. DOI: 10.1111/jace.18455

Authors' Short Biographies



Saeid Akrami

Saeid Akrami obtained a M.Sc. degree in Chemical Engineering, and he is currently a Ph.D. candidate in Applied Chemistry and Life Sciences at Nagoya Institute of Technology, Japan. His research interest is the development of highly-strained and high-entropy ceramics for CO₂ conversion and he is the author of several papers in this field.



Parisa Edalati

Parisa Edalati is currently a Ph.D. candidate in the Advanced Ceramics Research Center, Nagoya Institute of Technology, Japan. She was a visiting researcher at Kyushu University in 2019 before starting her Ph.D. study. She works on the design and synthesis of functional high-entropy alloys and ceramics for various applications including photocatalysis, biomedical application, hydrogen storage, and batteries.



Masayoshi Fuji

Masayoshi Fuji received his Dr. Eng. in 1999 and joined the Tokyo Metropolitan University, as a research associate in 1991. He was a visiting researcher at the University of Florida, USA, from 2000 to 2001. He joined the Nagoya Institute of Technology as an Associate Professor in 2002 and became a Professor in 2007. He is the editor-in-chief of *Advanced Power Technology* since 2019. His representative awards include the award from the Minister of Education, Culture, Sports, Science and Technology Japan in 2013, CerSJ award for academic achievements in ceramic science and technology in 2014, and the science award of the Society of Inorganic Materials, Japan in 2017.



Kaveh Edalati

Kaveh Edalati received his Ph.D. degree in Materials Physics and Chemistry from Kyushu University, Japan, in 2010. He currently serves as an Associate Professor at the International Institute for Carbon-Neutral Energy Research, Kyushu University, Fukuoka, Japan. His interests are the development of functional materials for carbon-neutral energy and hydrogen-related applications such as hydrogen storage and photocatalytic hydrogen generation and CO₂ conversion. He particularly utilizes the high-pressure torsion method to develop new functional materials. He is the author of over 150 journal papers and serves as the editor of several journals.